ChemCatChem

Concept
doi.org/10.1002/cctc.202500530

Chemistry Europe
European Chemical Societies Publishing

www.chemcatchem.org

Advanced Characterization of Proton Exchange Membrane Water Electrolyzers with Spatially-Resolved X-Ray Imaging

Leonardo Almeida De Campos,[b] Paolo Ciocci,[c] Johanna Schröder,[b] and Thomas L. Sheppard*[a, b]

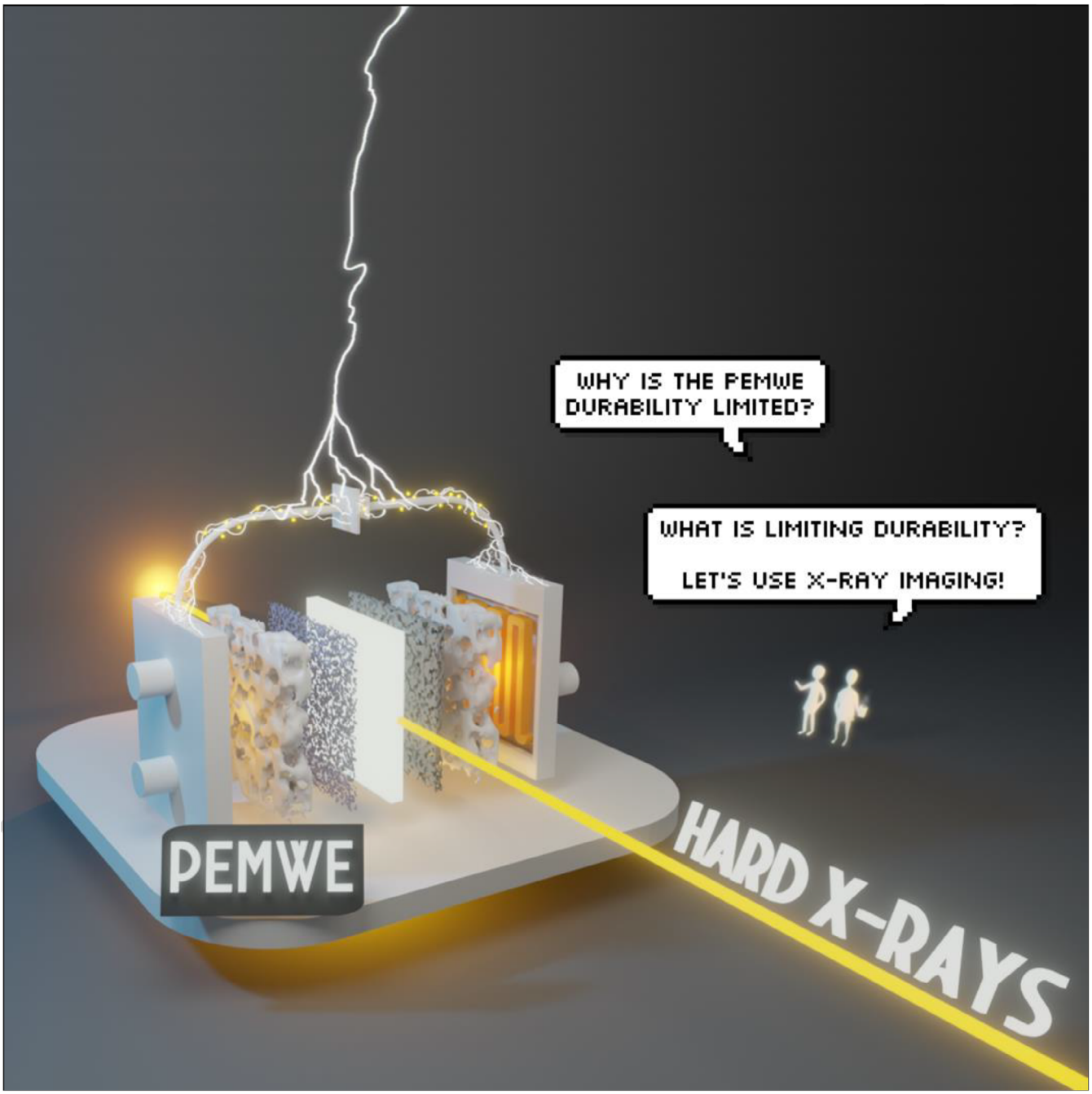

Electrocatalysis plays an increasing importance in mitigating chemical emissions, driving research on electrolysis for H_2 production. In this regard, it is a well-known challenge for the electrochemistry community that the key catalyst components for both the oxygen and hydrogen evolution reactions (OER, HER) are expensive noble metals that urgently require optimization, especially with respect to the degradation of proton exchange water electrolyzer (PEMWE). Optimized design and strategies to reduce the degradation of multiple components are essential to avoid misuse of these catalysts. For this purpose, visualizing chemical and structural changes at an intermediate scale and linking them with degradation processes is crucial to bridge the gap between process-scale PEMWE and lab-scale research, which generally focuses on model systems. In this review, we present multiple synchrotron case studies, from operando to ex situ, discussing the approaches currently used in the field over the last few years. With the depth discussion of strategies to spatially resolve intermediate-scale devices using synchrotron-based hard X-rays, we hope to guide further research in the electrochemistry community by adding specialized tools to the current set of characterization techniques.

1. Introduction

Given the finite nature of fossil fuels, electrochemical energy conversion technologies based on renewable sources are expected to be crucial in meeting current and future energy requirements with respect to sustainability, as well as independence and security.[1] One prominent approach for converting renewable energy into fuels and/or chemicals (e.g., hydrogen) is proton exchange membrane water electrolysis (PEMWE). PEMWE operates in a compact environment, offers rapid response capability, and provides high gas purity and robustness under various operating conditions.[2,3] Other devices based on proton exchange membranes, such as PEM fuel cells (PEMFCs) for producing chemical energy from H_2, PEM-based CO_2 electrolyzers for producing CO and hydrocarbons, and PEM electrolyzers for nitrogen reduction to ammonia, demonstrate further opportunities for sustainable chemical synthesis.[4–6]

Although PEM-based devices show great promise as established technologies, further research in the context of durability of catalyst and substrate materials is essential to optimize their performance and scalability. For instance, in PEMWE, the hydrogen evolution reaction (HER) and oxygen evolution reaction (OER) traditionally rely on noble metal catalysts like iridium (Ir) and platinum (Pt), which significantly raise production costs due to their limited supply.[7] Moreover, the commercial viability of PEMWE depends on the stability of catalyst-coated membranes (CCMs) for prolonged operational periods. To achieve this, it is important to understand and mitigate chemical or physical degradation pathways, such as the dissolution and/or migration of elements from catalyst layers, as well as membrane thinning phenomena.[8–10]

In design and operation of PEMWE-based devices, often a notable gap exists between fundamental academic research or laboratory-scale device testing compared to industrial demands, as highlighted by Tao and Zheng et al.[7] Academia tends to prioritize achieving maximum catalytic activity, minimizing noble metal usage, or developing noble-metal-free catalysts, while often deprioritizing factors such as cost, safety, and especially long-term durability. In this context, to better understand the challenges encountered with technical systems and improve the connection between academic research and real-life applications, a top-down approach assessing the structural complexity of real technical devices holds significant value as an alternative to lab-based materials discovery or trial-and-error. However, comprehensive studies of technical devices depends on appropriate characterization methods which properly address the system complexity in a spatially-resolved and structurally representative manner, in particular under operating conditions. An effective pathway to achieve this could involve X-ray synchrotron-based technologies, particularly X-ray imaging, employing a multiscale approach to understand structural and chemical aspects of PEM devices under operation.[11]

This article highlights developments in characterization which can be used to enhance our understanding of PEMWE devices on the technical scale. A toolbox of methods based mainly on X-ray imaging with synchrotron radiation are discussed, covering both current works and future prospects. Studies which effectively address the multiscale complexity of

[a] Prof. Dr. T. L. Sheppard
Institute of Chemical Technologies and Analytics, TU Wien, Getreidemarkt 9/164, Vienna 1060, Austria
E-mail: thomas.sheppard@tuwien.ac.at

[b] L. Almeida De Campos, Dr. J. Schröder, Prof. Dr. T. L. Sheppard
Institute for Chemical Technology and Polymer Chemistry, Karlsruhe Institute of Technology, Engesserstraße 20, Karlsruhe 76131, Germany

[c] Dr. P. Ciocci
Institute of Catalysis Research and Technology, Karlsruhe Institute of Technology 76344, Eggenstein-Leopoldshafen, Germany

Abbreviations: 2D XRF, 2D X-ray fluorescence; ALS, Advanced light source; APS, Advanced photon source; CL, Catalyst layer; CCMs, Catalyst-coated membranes; CT, Computed tomography; FOV, Field of view; FIB-SEM, Focused ion beam microscopy; FC, Fuel cell; TXM, Full-field transmission X-ray microscopy; GDL, Gas diffusion layer; HER, Hydrogen evolution reaction; Ir, Iridium; MEA, Membrane electrode assembly; MPLs, Microporous layers; NSLS-II, National synchrotron light source II; OCV, Open circuit potential; OER, Oxygen evolution reaction; Pt, Platinum; PTE, Porous transport electrode; PTL, Porous transport layer; PEMWE, Proton exchange membrane water electrolysis; PXCT, Ptychographic X-ray computed tomography; PyXL, Ptychographic X-ray laminography; ROI, Region of interest; SEM, Scanning electron microscopy; SSRF, Shanghai synchrotron radiation facility; SLAC, Stanford linear accelerator center; SLS, Swiss light source; Ti, Titanium; TEM, Transmission electron microscopy; TPCA, Triple-phase contact area; XANES, X-ray absorption near edge structure.

PEMWE devices, as well as in situ/*operando* technologies for deriving structure–activity relations, are exclusively in focus. The overarching goal of such studies is to pinpoint the structural and chemical stability of PEM devices for long-term industrial usage. In achieving this, such information can guide the design of future PEM systems with greater performance and durability, which better meet the needs of industry.[12,13]

2. From Bulk Analysis to Spatially-Resolved Catalyst Characterization

Within catalysis, there are two broad approaches to understand the structure and chemistry of catalytic materials and processes, which, in the authors' opinion, can be generally divided into model scale and process scale. The model scale approach includes the study of model systems, surface science, fundamental kinetic studies, high resolution imaging (e.g. electron microscopy), and related methods where the system is in a form or environment far from technical application. The process scale approach includes scaled-up analysis of conversion, yield, and selectivity, kinetics in the context of chemical reaction engineering, reactor simulations and modeling, as well as laboratory-scale study of technical catalyst materials without considering nanoscale material degradation phenomena. It is a notable but well-known contradiction, sometimes referred to as the pressure and/or materials gap,[14] that model systems are often ideal for characterization purposes yet may not be representative of real-world technical scenarios, and vice versa considering the challenges with performing characterization on the scale of large chemical reactors. An alternative approach, which in the context of electrocatalysis may be considered as "device-like" conditions,[15] aims to balance studying intermediate scale systems or realistic process conditions, while maintaining the precision and sensitivity of high-performance characterization methods. The development of synchrotron radiation has further expanded the possibilities of characterization from traditional ex situ and post-mortem analysis of bulk systems to in situ/*operando* analysis. In situ techniques probe the catalyst structure under conditions relevant to its function, whereas *operando* methods go a step further by simultaneously measuring the catalyst structure and its performance metrics—i.e., activity and selectivity—under model or realistic reaction conditions.[16] However, the precise definition of *operando* is still a matter of debate within different communities.[17]

In the context of device-like conditions, spatially-resolved analysis methods are particularly valuable in obtaining accurate physicochemical information. Such methods complement common bulk analysis by providing more meaningful data in which physical structure is locally correlated to chemical properties on the device level, thereby increasing the transferability of knowledge from model to process scale systems. X-ray imaging with synchrotron radiation is highly relevant for spatially-resolved characterization of device-scale systems, due to high penetration

Leonardo Almeida De Campos is a PhD student at the Institute for Chemical Technology and Polymer Chemistry (KIT, Germany), working with Prof. Sheppard and Prof. Grunwaldt. He holds an MSc in chemical engineering (UEM, Brazil, 2022) and has worked on heterogeneous catalysis for green diesel production and the characterization of proton exchange membranes for water electrolysis. His current research focuses on synchrotron-based multiscale imaging for sustainable catalysis.

Paolo Ciocci is currently postdoctoral researcher at Institute of Catalysis Research and Technology at Karlsruhe Institute of Technology (KIT, Germany) at AK Grunwaldt. He owns a PhD in physical and analytical chemistry from Université Paris Cité focused in developing protocols for operando microscopy applied to nanoelectrochemistry. Currently, he works on synthesis of new catalysts for water electrolysis and on their operando characterization on device-scale by synchrotron-based techniques.

Johanna Schröder is a KIT Junior Research Group Leader working on electrocatalytic operando characterization with a focus on water electrolysis. After receiving a PhD at University of Bern, she worked as a postdoctoral researcher at Stanford University and SLAC National Accelerator Laboratory before she moved to Karlsruhe and KIT.

Thomas L. Sheppard is full professor of Applied Solid State Chemistry at TU Wien (2025) and guest scientist at Karlsruhe Institute of Technology where he leads the working group "X-ray Microscopy in Catalysis". Research interests are mainly in heterogeneous catalysis and related functional materials. Multimodal and multiscale characterization often makes use of synchrotron radiation (X-rays), with a strong focus on spatial- and time-resolution, imaging methods, in situ/operando methods, and addressing the materials gap between model and technical scale systems.

through matter and the variety of contrast modes available.[18,19] Intermediate systems can be studied to reveal structural properties or chemical gradients such as elemental distribution of dispersed parts of the catalyst layers[20] or even oxidation states through agglomerate structures in PEMWEs,[21] as highlighted in the following sections.

2.1. Scope of this Paper

We aim to present to the electrochemistry community various application cases of PEMWE at a technical scale, demonstrating the value of advanced characterization using synchrotron-based X-ray imaging. Although other studies have focused on characterizing specific components of PEMWE, or have not been exclusively dedicated to spatially-resolved synchrotron-based X-ray imaging,[22–24] this work bridges both by offering a broader perspective relating to the multiple components present in PEMWE systems. The authors note the significant prior literature of Zenyuk et al.,[11,25,26] whose extensive research has provided valuable insights into tomography applied to electrochemical devices covering a wide range of applications, including PEMFCs, batteries, and PEMWE. Although the present paper specifically focuses on PEMWE, readers seeking further information on different devices and techniques beyond spatially-resolved hard X-ray imaging are encouraged to check the above literature.

To provide a clear overview of the structure, Table 1 summarizes each application case, the technique used, and the corresponding synchrotron facility and beamline at which PEMWE characterization was performed. Additionally, the key features of interest and a brief summary of the main observations from each study are included.

2.2. Current PEMWE Structure and Device Composition

Conventionally, PEMWE can be described as shown in Figure 1,[23] in which three main components are present: a membrane electrode assembly (MEA), porous transport layers (PTLs), and bipolar plates. A MEA is based on a solid electrolyte membrane (e.g., Nafion-based membranes) with a catalyst layer (CL) for the anode (e.g., Ir/IrO_2-based catalyst) and another CL for the cathode (e.g., Pt/C-based catalyst), therefore promoting OER and HER, respectively. Between the bipolar plates and the MEA, PTLs are added to enhance gas and liquid phase diffusion properties, being crucial as well for electric conduction between the electrodes (electrocatalytic layer) and the bipolar plates. For consistency, the transport layer at the cathode, also called gas diffusion layer (GDL), is here included as a PTL. For anodic and cathodic bipolar plates, carved grooves are present in order to evenly distribute water over the porous transport layers and for the discharge of the generated gases. Finally, it is important to note that two main components for PEMWE MEAs are frequently discussed.[30,37,38] The first is the CCM approach, in which the CLs are directly coated onto the solid electrolyte membrane, followed by assembly with PTLs. The second component involves depositing the CLs onto the PTLs, forming a porous transport electrode (PTE), which is then assembled with the solid electrolyte membrane. This generally relies on mechanical compression or bonding to ensure efficient proton conduction and structural integrity.[39]

Among conventional MEA and PEMWE cells, multiple options for different solid electrolyte membranes (Nafion 115/117, hydrocarbon-based polymers, etc.), electrocatalytic layers (for the anode: Ir–tungsten, laminar Ir, Co-RuIr, etc.), and PTLs (carbon, fiber or sintered titanium – Ti, etc.) have been tested as alternatives to benchmark systems (e.g., anodic catalysts IrO_2/TiO_2, 75 wt% Ir) for improving the design and durability.[23,40,41] It is a considerable challenge to overcome benchmark materials such as Nafion ionomer/membrane or Pt/C and Ir oxide catalysts since they are quite established commercially and sometimes even considered irreplaceable due to their strong performance. Although multiple novel formulations appear every year, in many cases the central challenge preventing industrial uptake of viable PEMWE cells is long-term stability. For example, under high potential PTLs based on Ti can be passivated and corroded, turning into oxidized Ti and further possibly moving into the solid electrolyte as suggested in our previous work,[20] and consequently decreasing catalytic activity and conductivity.[42,43] A similar challenge is that under harsh conditions or long operation times the precious-metal elements (Ir and Pt) can either dissolve from the CL into the water flow, or migrate toward the solid electrolyte.[20] In summary, understanding system degradation in technical devices is a considerable challenge, but probing and revealing such degradation mechanisms in tandem with synthesis improvements could efficiently motivate future PEMWE designs.

2.3. Probing PEMWE Structure and Chemistry: The Multiscale Problem

From literature,[7,11,22] PEMWE optimization studies suggest that studying each system components (e.g. PTLs, CLs, or solid electrolyte) is crucial to improve commercial affordability, stability, and effectiveness. Nevertheless, it is important that chemical and morphological properties are discussed based on different techniques and components of MEAs as a whole, then creating a fertile ground for new strategies to improve the construction of electrolyzers. In view of the aforementioned structure of MEAs, electrolyzers require electrocatalysts and porous electrodes, in which the main goal is to increase the catalyst active surface area. Since commonly-used catalysts together with PTLs present a complex and hierarchical structure, multiple degradation phenomena (e.g., pore collapse, catalyst dissolution, and aggregation) can be evaluated from nano up to centimeter scale. Commonly, morphology characterization is done either by electron microscopy techniques such as scanning electron microscopy (SEM), focused ion beam microscopy (FIB-SEM), and transmission electron microscopy (TEM), or by scanning probe techniques such as electrochemical atomic force microscopy (AFM) or electrochemical scanning tunnel microscopy (STM).[44–46] However, limitations such as sample preparation (often invasive and destructive), environment conditions (e.g., vacuum required for SEM and TEM), and sample size (constrained to small regions of

Table 1. Articles cited dealing with structural evaluation of PEM systems using synchrotron-based X-ray imaging.

Ref./ Year	Method	Feature of Interest	Observation	Analysis[g]	Beamline	Pixel/Voxel Size[n]
[27] 2018	XCT[a] (microCT)[(1)] and 2D radiography[(2)]	PTL (carbon), CL (IrxRuyOz) and PTL/CL	Ir migration from anode to PTL	In situ [(1,2)]	2-BM (APS)[h]	1.33 µm
[28], 2021	XCT (microCT) and 2D radiography	Ti-based PTL (fiber)	Bubble nucleation and transport within PTL (stained water)	*Operando* [(1,2)]	TOMCAT (SLS)[j]	2.75 µm
[29], 2021	XCT (microCT) and 2D radiography	Ti-based PTL (multiple configurations)	Bubble nucleation for end-of-life loadings	*Operando* [(1,2)]	2-BM (APS)	1.73 µm
[30], 2022	XCT (microCT) and 2D radiography	Ti-based PTLs or PTE and CL	Cat. agglomeration on CCM versus better CL conformation for PTE	*Operando* [(1,2)]	8.3.2 (ALS)	1.16 µm
[31], 2023	XCT (microCT) and 2D radiography	MPL	Optimized MPL increased oxygen distribution. MPL/CL was not resolved.	*Operando* [(1,2)]	2-BM (APS)	0.64 µm
[32], 2019	TXM[b] (nanoCT)	CL	Nonuniformities and spacing among CL agglomerates	Ex situ	18-ID (NSLS II)[k]	30 nm
[33], 2023	TXM (nanoCT)	CL	CT of CL structure allowed simulation of ionomer mesh	Ex situ	18-ID (NSLS II)	30 nm <
[34], 2024	TXM (nanoCT)	CL	Higher porosity when tuning agglomerates with octadecanethiol	Ex situ	BL18B (SSRF)[l]	30 nm
[21], 2022	2D TXM/XANES[c]	CL	Ir oxidation maps under varied experimental conditions	Ex situ	6–2c (SLAC)[m]	23.3 nm
[20], 2024	2D XRF[d]	CLs, Nafion membrane	Metal migration from anode/cathode into membrane	Ex situ	microXAS (SLS)	1 µm
[35], 2023	PXCT[e]	CL/Ionomer	Resolved ionomer/catalyst structure	Ex situ	cSAXS (SLS)	16.4 nm
[36], 2024	PyXL[f]	CL/Ionomer	Poor contrast for wet CL (Ionomer/water)	Ex situ	cSAXS (SLS)	35 nm <

[a] XCT, X-ray computed tomography;
[b] TXM, Full-field transmission X-ray microscopy;
[c] 2D TXM/XANES, 2D full-field transmission X-ray microscopy/X-ray absorption near edge structure;
[d] 2D XRF, 2D X-ray fluorescence;
[e] PXCT, ptychographic X-ray computed tomography;
[f] PyXL, ptychographic X-ray laminography;
[g] Operando experiments considered O_2 evaluation without directly quantifying it, except imaging itself, while measuring activity by other means;
[h] Advanced Photon Source (APS), Illinois, USA;
[i] Advanced Light Source (ALS), California, USA;
[j] Swiss Light Source (SLS), Villigen, Switzerland;
[k] National Synchrotron Light Source II (NSLS II), New York, USA;
[l] Shanghai Synchrotron Radiation Facility (SSRF), Pudong, China;
[m] Stanford Linear Accelerator Center (SLAC), California, USA;
[n] Pixel/voxel size is not equivalent to image resolution.

Chemistry Europe
European Chemical Societies Publishing

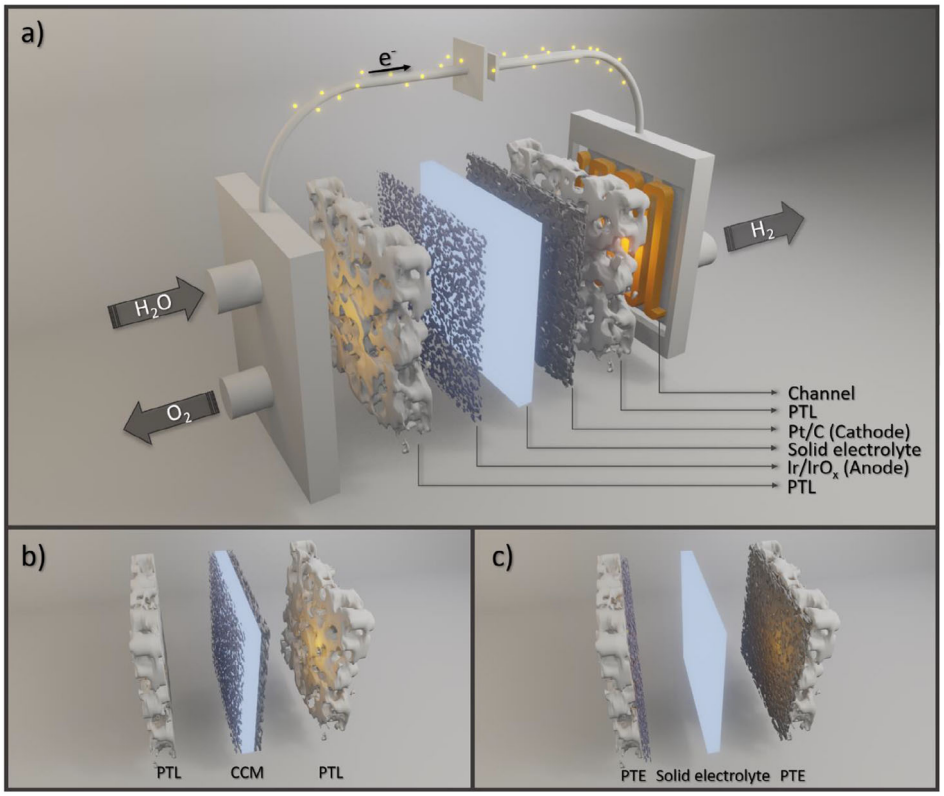

Figure 1. PEMWE cell compact view structure, a) complete cell, b) CCM and PTL components, and c) PTE and solid electrolyte components.

interest due to beam attenuation) are typically encountered. This limited possibility to analyze representative regions of interest is a significant drawback in associating the different components of a PEMWE device for durability evaluation, or when performing in situ or *operando* measurements.[47]

To allow a 3D analysis of the catalyst layer and the whole MEA, computed tomography and synchrotron-based X-rays can be broadly applied to investigate PEMWE systems and individual components across numerous length scales. This is particularly due to the high penetrating power of hard X-rays, high photon flux of synchrotron light sources, and flexibility in the design and implementation of X-ray imaging setups in terms of spatial resolution, contrast mode, and sample environment. As seen in Figure 2, investigation of PEMWE structures can be correlated with complex reaction behaviors from a multiscale perspective by using different techniques (e.g., microCT, nanoCT, ptychography). In this approach, technical devices can be analyzed from the perspective of understanding mass transport phenomena, followed by the evaluation of mechanical degradation in CLs, PTLs, or PTEs due to bubble nucleation or sintering. Additionally, as the scale decreases, high resolution studies on agglomerates and multiple contrasting phases within catalyst aggregates provide valuable information into PEMWE design, which is only feasible using synchrotron-quality data.[11]

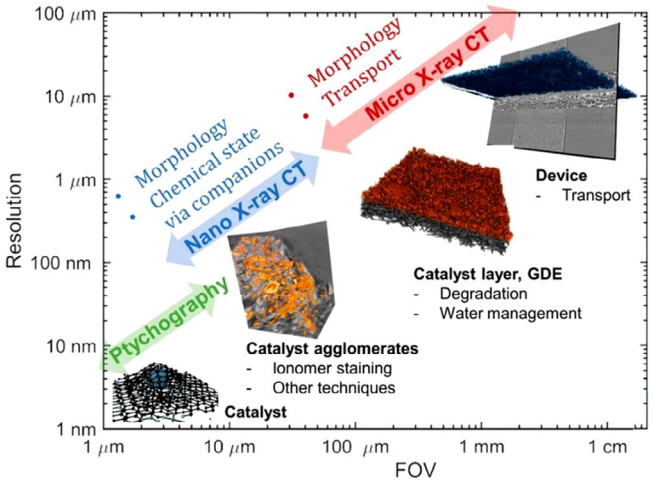

Figure 2. Multiscale scenario for the evaluation of PEM components: From technical devices to catalyst aggregates, multiple challenges can be addressed using hard X-ray imaging. Hereby, the authors aim to present application scenarios with a multiscale approach, ranging from the microscopic level (a few microns) to the macroscopic level (centimeter scale). Notably, most images are actual data based on real CT scans. Reprinted with permission from Ref. [11]. Copyright 2023 American Chemical Society.

2.4. Structural Evaluation: Spatially-Resolved Analysis

Due to the porous and tortuous pathways involved, mass transport of fluid phases and removal of gas product are relevant phenomena from micrometer (hundreds of microns) to centimeter scale. This is especially relevant during long-term operation,[37,48] in which catalyst layers can change by thinning, pore collapse, and electroactive material detachment, or even suffer from bubble blockage, disconnecting the active sites from the electrolyte.[49,50] For measurements between tens of microm-

eters and nanometers, agglomerates of support and catalysts can be formed and further studied by X-ray tomography in order to evaluate size distributions over time, since performance and operation are closely dependent on the morphology of these sites.[33,34] Here X-ray based techniques for PEMWE morphology characterization are discussed for different application scenarios and techniques based on the spatial resolution which can be obtained in the measurement.

2.4.1. Microcomputed Tomography and Radiography

PEMWE devices consist of composite porous solids packed within a confined cell. The nature of the pore structure in each component can be expected to play a crucial role in the overall device performance. Understanding structural degradation or morphology evolution in terms of transport processes within PEMWE is therefore important in order to rationalize device performance. Ideally, this can be extended to develop new devices, or to overcome limitations of current existing devices that are often burdened with high costs for industrial operation.[22,43,51] With this said, it is also notable that morphology evolution can be correlated with the complexity of two-phase transport processes within PEMWE. For example, bubble nucleation can take place affecting the structural integrity of CL or PTL, since oxygen can be found either in gas phase (bubbles) or dissolved in water. To ensure high performance, the removal of this bubble phase is crucial to avoid blockage of the catalyst layer surface, which can otherwise result in decreased catalyst activity. In literature, models have been reported to understand bubble evolution,[52–55] though as with any model, correlation to real data (e.g., provided by X-ray imaging) is important for validation and optimization.

X-ray imaging methods have been evolving (improving time and spatial resolution) to allow *operando* measurements to take place while capturing morphology changes of electrochemical devices. In general, synchrotron microCT works by directing intense, monochromatic X-rays from a synchrotron source through a sample while rotating it in a fixed axis.[56] During this process, a detector captures 2D projections (at different angles), which later are reconstructed into a 3D model of the interior structure using computational algorithms. The term radiography as an imaging technique in materials science typically relates to acquiring the 2D projection images noted above, which are normally (though not always) based on differences in X-ray absorption contrast. In other words, tomography is constructed from a series of radiographic projections. This section highlights literature on PEMWE systems using microCT and radiography, which can both probing the physical structure of different components, as well as investigate mass transport phenomena.[57]

As an early case study, Leonard et al.[27] investigated the morphology evolution of PTLs combining synchrotron-based microCT and X-ray radiography as nonintrusive 3D and 2D imaging techniques. Their experiment utilized a model carbon-based PTL in the anode side, in order to ensure enough X-ray transparency while simulating PTL properties. It should be noted that in PEMWE systems Ti PTLs are preferable for the anodic compartment due to their higher durability under harsh reaction conditions. Although carbon-based PTLs corrode at potentials lower than Ti PTLs, they are a common compromise when trying to simulate all properties from these materials for model systems.[22] From that, reference scans (microCT followed by radiography for 30 s with 100 ms per projection) were collected under open circuit potential (OCV) followed by in situ radiography experiments (current density holds at OCV, 50, 100, and 200 $mA.cm^{-2}$) and later tomography scans at longer constant current holds at 50 or 200 $mA.cm^{-2}$. This enabled the identification of increasing amounts of catalyst $Ir_xRu_yO_z$ from the anode depositing in the PTL region. When increasing the current, this apparent detachment of electroactive material from the CLs increased, exposing significant morphological changes in the PTL region and further degradation of the CL. An overlay of the tomographic scan of the initial (gray) and under operation state (blue and red) can be seen in Figure 3c) where the anode catalyst partially moves into the PTL layer.

Despite the fact that model materials (e.g., carbon) replicate essential PTL structural characteristics such as pore sizes and throats, applying these findings to real-world PEMWE remains challenging as key interactions such as oxygen production, current density, and oxygen saturation cannot be transferred from simplified models to technical solutions, e.g., Ti-based PTLs. To replicate realistic conditions, De Angelis et al.[28] used Ti-based PTLs while measuring two-phase flow (oxygen/water) and introducing a solution to better visualize oxygen diffusion under microCT/radiography *operando* analysis. Typically, the high X-ray absorption of Ti-based PTLs should pose a significant challenge for visualizing contrast between the much less absorbing water and oxygen phases. Here Ti-fiber PTLs and a 5 wt% iodic acid–water electrolyte (stained water) were used to enhance differentiation between gas/liquid and solid as shown in Figure 4. High-resolution microCT imaging achieved a pixel size of 2.75 µm, a field of view (FOV) of $5.5 \times 5.5\ mm^2$, and a temporal resolution of 1.4 s per tomogram. In their findings, it was possible to observe a capillary-driven flow regime with oxygen saturation increasing near the PTL/catalyst layer interface when applying higher current densities. At low current densities, oxygen pathways appeared as isolated clusters, merging into larger, better-connected networks as current density increased. Finally, the analysis of pore network and water distributions with this microCT technique showed that oxygen initially occupied larger pores, with smaller pores becoming accessible at higher current densities. This study offered critical insights into the interplay between pore morphology and oxygen transport in a structure more representative of industrially applied PEMWE systems.

In a later study to simulate end-of-life loadings and highlight possible degradation pathways within the PTL not described previously in literature, Peng et al.[29] investigated how five different PTLs (differing in porosity, tortuosity and thickness, Ti fiber diameter of 20 µm) would affect the PEMWE operation at an ultralow catalyst loading (0.05 $mg_{Ir}.cm^{-2}$). Their PEMWE testing followed a protocol reported in previous work,[58] ensuring no significant variation in catalyst layer loading for each membrane, so that differences in performance could be directly related to different PTL properties. MicroCT was employed to explore mass transport properties, also evaluating different regions such as

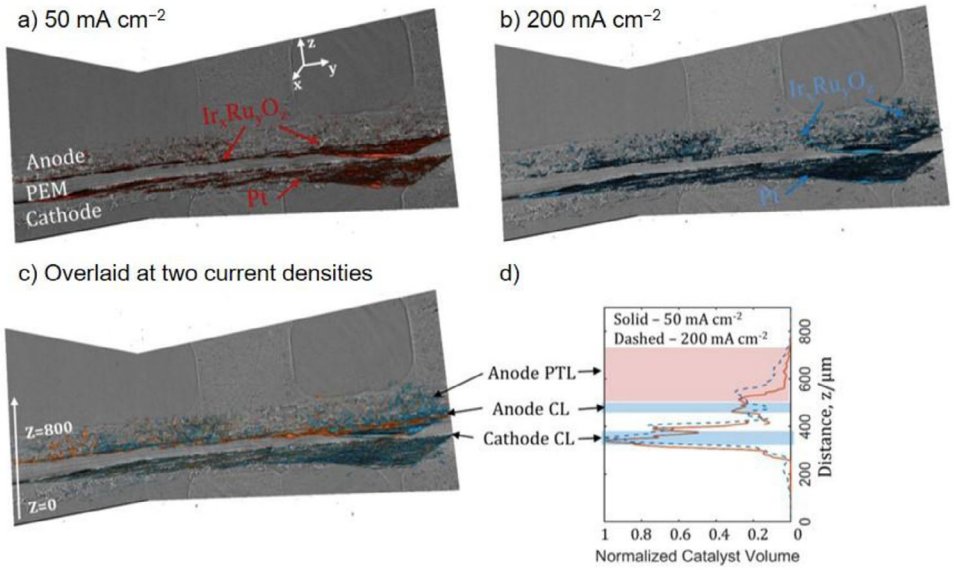

Figure 3. Volume rendering of tomogram cross-sections of the electrocatalyst is shown by fresh catalyst overlapped by longer constant current holds at a) 50 and b) 200 mA.cm^{-2}. Combined volume rendering from a) and b) is shown by c). Volume fraction of electrocatalyst (normalized in such a way that the maximum value is one) versus distance across the cell for two current densities is shown by d). Adapted from Ref. [27]. Copyright (2018), with permission from Elsevier.

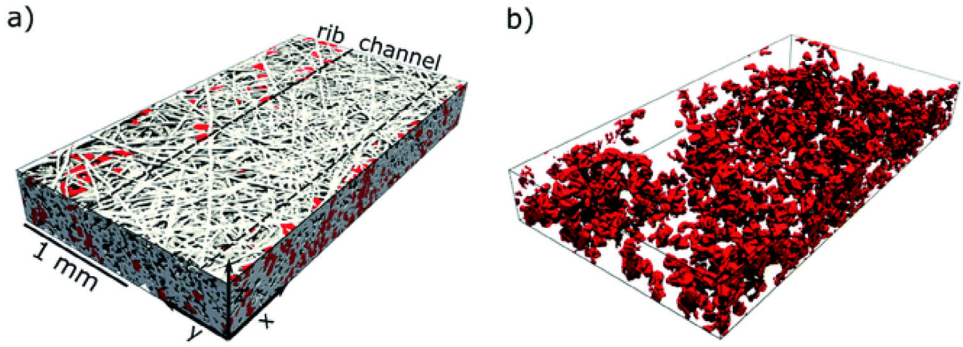

Figure 4. 3D renderings of the PTL region for the current density of 0.5 A cm^{-2}. In (a) the PTL fibers are shown in gray and the oxygen phase in red; (b) 3D rendering of the oxygen pathways inside the PTL. Reproduced from Ref. [28] with permission from the Royal Society of Chemistry.

CL/PTL, middle region of PTL (mid-PTL), and PTL/flow field channel (PTL/channel) at a fixed current density of 3 A.cm^{-2} (see Figure 5b). By radiography, results suggested oxygen is mostly present in the CL/PTL interface, decreasing toward the direction of the PTL/channel layer (see Figure 5a). The authors highlighted that the lower oxygen removal resistance contributed to an increased water permeation to the catalyst active sites and to lower kinetic overpotentials. In conclusion, changes in PTL bulk properties were observed to impact PEMWE oxygen transport. This highlights the importance of understanding interface structures at ultralow catalyst loadings, which was only possible by combining MicroCT and radiography for oxygen transport evaluation.

As for the evaluation of the CL/PTL distinct interfaces, Kulkarni et al.[30] discussed the performance of PEMWE by varying catalyst loadings, simultaneously varying the catalyst layer composition (different Ti-based PTLs, sintered and fiber) and MEA preparation techniques (PTE or CCM plus PTL). Tomography revealed that catalyst agglomeration increased with loading in CCMs, while using carbon-based PTEs the catalyst conformed to the PTL surface during coating, distributing it homogeneously (Figure 6). The index triple-phase contact area (TPCA), variable based on the surface area of the catalyst phase per the intersection surface area of PTL plus Nafion (calculated with tomographic information), was used to measure the area of deposited catalyst contacting the Nafion membrane. This essentially translates to how "accessible" the catalyst is for OER. It was found that an increase in catalyst loading together with different catalyst morphologies would directly impact this index, later demonstrating that even though catalyst agglomeration was noticed for highly loaded sintered CCMs, this component had the biggest TPCA and highest double-layer capacitance, leading to lower overpotentials and better efficiency for OER. Regarding the PTL structure, a crucial role was played in the oxygen transport, as the sintered PTLs exhibit smaller, uniform pores allowing better oxygen distribution, while fiber PTLs had larger, uneven pores causing oxygen channeling. In addition, radiographic imaging confirmed that oxygen indeed followed

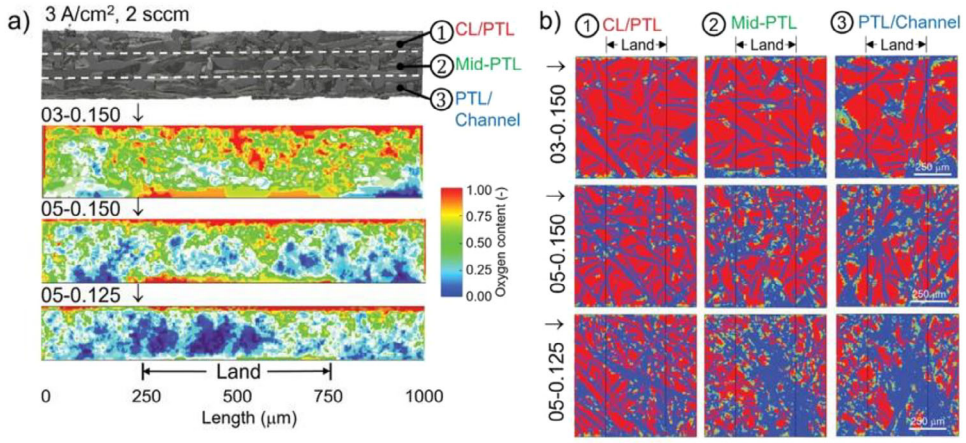

Figure 5. Tomographic summary plots detailing the oxygen distribution at interface of CL/PTL, middle interface of PTL, and interface of PTL/flow field channel for different samples. a) In-plane oxygen distribution of these samples, b) through-plane oxygen distribution at each interface. Adapted from Ref. [29] and used under the Creative Commons License (CC BY 4.0).

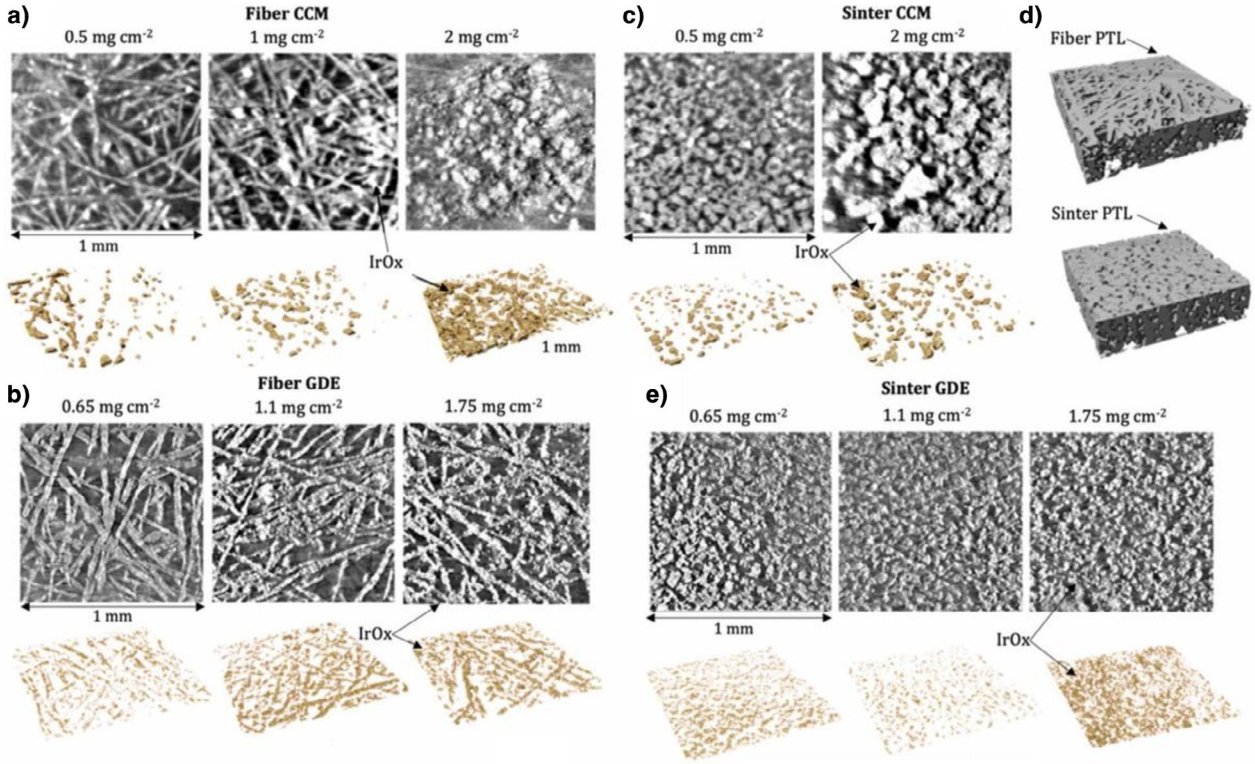

Figure 6. 2D reconstruction and 3D renderings of catalyst and PTLs in different cells obtained from x-ray tomography a) Fiber CCM 0.5, 1, and 2 mg.cm^{-2}. b) Fiber GDE 0.65 and 1.1and 1.75 mg.cm^{-2}, c) sintered CCM 0.5 and 2 mg.cm^{-2}, d) sintered GDE 0.65 and 1.1 and 1.75 mg.cm^{-2}. e) 3D renderings of fiber and sintered PTLs. Reprinted from Ref. [30]. Copyright (2022), with permission from Elsevier.

preferential channels through the PTL. At high current densities, slug flow formation in the channels enhanced mass transport, also resulting in reduced overpotentials. Tomography-based 3D modeling later revealed that lower catalyst loadings would also lead to limited oxygen pathways, particularly in fiber PTLs.

The effect of adding microporous layers (MPLs) on PTLs to upgrade the anodic interface and oxygen transport properties was later described by Kulkarni et al.[31] and Schuler et al.[59] MicroCT and radiography were employed by Kulkarni et al.[31] to determine morphology and oxygen distribution on the interface of sintered Ti-based PTLs (as baseline without MPL) and with Ti-based MPLs on top (20 versus 58 μm). Even though it was difficult to resolve oxygen within the MPL, the contribution of microCT and radiography is noteworthy since it allowed to visualize the gas content within PTLs. Results showed that MPLs doubled the PTL contact point density, consequently also improving the contact homogeneity of the PTL with

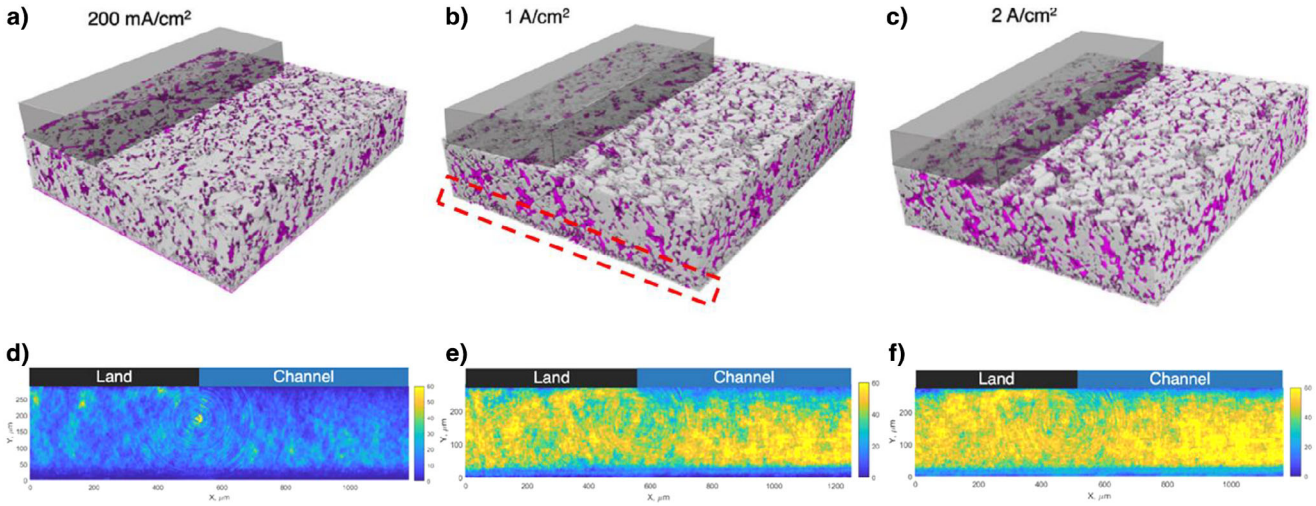

Figure 7. (a–c) 3-D volume renderings of PTL and MPL and (d–f) corresponding 2-D averaged projections (Z-projects) at 200 mA.cm^{-2}, 1, and 2 A.cm^{-2}, respectively. The color bar for Z-projects represents the % of oxygen normalized to pore volume. Oxygen could not be resolved within the MPL (dashed red box in b); However, it allows formation of better and more well-connected pathways for oxygen removal through the macro porous layer. Reprinted with permission from Ref. [31]. Copyright 2023 American Chemical Society.

the CL compared to samples without MPLs. Furthermore, the authors stated that the presence of MPLs can reduce mechanical deflections due to more even pressure distribution at the contact points (see Figure 7 for different applied currents). Imaging also revealed that MPL samples had higher pore volume utilization at any given current density, which directly correlated with improved oxygen removal efficiency. Additionally, bubble point measurements indicated that increasing MPL thickness led to higher bubble point pressures (pressure for gas to break through the liquid-filled pores) then decreasing mass transport of oxygen. For thinner MPLs, oxygen transport is in through plane direction, while for thicker MPLs, in-plane oxygen transport can isolate the catalyst from water. The 3D analysis demonstrated that sintered PTLs without MPLs exhibited capillary fingering as the dominant oxygen transport regime, MPLs suppressed this behavior and promoted viscous fingering, allowing more efficient oxygen removal. Finally, durability tests over 1000 h also reported that the thinner MPL provided the best performance, whereas the thicker MPL led to mass transport limitations. The study also found that at low catalyst loadings (0.1 mg/cm^2), MPLs significantly improved durability, highlighting their importance in maximizing catalyst utilization and minimizing degradation. To overcome resolution and contrast limitations for resolving oxygen, additional characterization with better spatial resolution would be of great use for this application, enabling access to information in the region of the CL/MPL/PTL assembly.

Considering the above case studies using microCT and radiography to investigate PEMWE systems at the micrometer scale, successfully evaluation of various phenomena under *operando* or in situ conditions is noteworthy. These include species migration from the CL to the PTL, bubble nucleation and transport across different layers and interfaces (e.g., CL/MPL/PTL), catalyst loading optimization for specific configurations (PTE or CCM), and assessment of different transport layer types (e.g., Ti-fiber or sintered). Additionally, numerous morphological observations (e.g., pore structure, pore collapse, and channeling) of the various PEMWE components were made.

Such observations, especially when conducted *operando* or in situ, are challenging without microCT and radiography, as these methods provide both spatial and temporal resolution along with noninvasive depth contrast. All these factors ensure that X-ray imaging studies are generally representative under realistic or device-like conditions. As an outlook, given the wide range of applications for microCT, it is important to establish standardized imaging protocols for PEMWE, especially at the scale of technical devices. These protocols should not necessarily be for routine experiments only, but should facilitate better organization and faster identification of the most suitable techniques to address different scientific questions corresponding to the structure, durability, and related properties.

2.4.2. Nanocomputed Tomography

The characterization of degradation mechanisms (such as mechanical stress, dissolution or migration, and oxidation) and multicomponent interactions (e.g., Nafion/CL/PTL) within PEMWE, ranging from hundreds of micrometers to the centimeter scale, can be visualized using X-ray microtomography or radiography as shown above. However, observations are only feasible up to a certain resolution limit of the measurement, noting that there is a distinction between pixel/voxel size of the detector/microscope and actual resolution of the final images.[60] Investigating phenomena at the micrometer scale or below requires higher resolution, e.g., insufficient resolution may prevent the clear visualization of bubbles forming within a thin MPL layer[32] or the proper imaging of the CL, since electrocatalysts are usually synthesized as nanoparticles with sizes varying from 1 to few hundred nanometers.[61] To cover this issue, synchrotron-based nanoCT offers higher resolution, but typically at the expense of a smaller FOV.[18] It should be noted that due to the compromise between FOV, time, and target

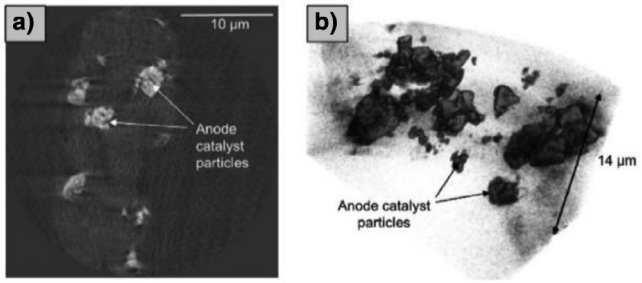

Figure 8. Dispersion of the CCM anode catalyst layer particle in two views: (a) tomographic cross-section showing anode catalyst particles and (b) a volume rendering showing the in-plane isolation of catalyst particles. Reproduced from Ref. [32] with permission from the Royal Society of Chemistry.

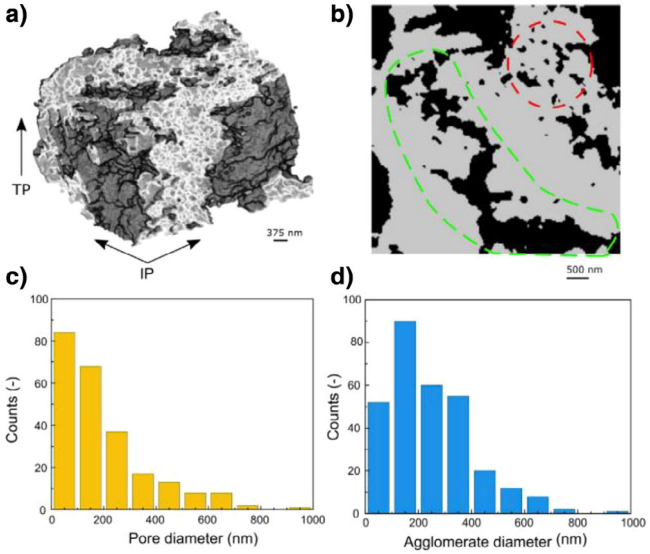

Figure 9. Structural characterization of iridium-based catalyst. (A) 3D reconstruction of the iridium-based catalyst obtained via synchrotron TXM acquired from the Full-Field X-ray Imaging beamline (18-ID) of NSLS-II. Colors are used for visualization purposes only. The scale bar represents 375 nm. (B) A cross-sectional image of the iridium-based catalyst revealing the wide range of pore sizes. The scale bar represents 500 nm. (C and D) A pore size distribution (C) and an agglomerate size distribution (D) of the iridium-based catalyst. Reprinted from Ref. [33]. Copyright (2023), with permission from Elsevier.

resolution in imaging studies, nanoCT by default operates on smaller sample volumes than are possible with microCT. This should be carefully balanced against the representativeness of the measurement, similarly to the use of electron microscopy. Furthermore, it is also important to keep in mind that nanofocused X-rays are more prone to provoke beam damage due to the higher photon flux incident on the sampling area, although these effects can be studied with control experiments and/or mitigated, as described elsewhere.[62]

An effective demonstration of resolution limits is the study by Leonard et al.,[32] which investigated the interfacial contact between transport layers and catalyst layers in using microCT, radiography and nanoCT. Here PTE and CCM components for MEA were studied, while also varying the type of Ti transport layer (sintered and fiber) for the CCM at two different current densities. Among their results, microCT analysis revealed that both CCM and PTE structures could be resolved at a certain degree, with the CCM exhibiting greater homogeneity, leading to improved contact between the electrocatalyst, membrane, and PTL. This consequently resulted in better performance, although catalyst clusters were present in both configurations. Despite these observations, the resolution of microCT was insufficient to resolve the catalyst layer within the CCM. To address this issue, nanoCT was employed, achieving a resolution of approximately 30 nm, allowing the identification of nonuniformities in the catalyst layers, revealing spacing in-between catalyst agglomerates within the region of interest (Figure 8). Furthermore, these findings raised new questions about catalyst connectivity on the anode side due to conformation of agglomerates through the CL.

Despite the extensive literature on structure optimization, little attention has been given to the direct observation and characterization of the catalyst layer of PEMWEs at the nanoscale. Following the questions left by Leonard et al.,[32] Lee et al.[33] evaluated the porous structure of Ir-based catalyst layers using nanoCT. With a pixel resolution of 30 nm, the pore structure of an Ir-based sample (5.55 × 5.55 × 3 µm) was resolved, revealing the presence of pores ranging from tens of nanometers to a few microns as shown in Figure 9. Although the authors identified smaller pores on the scale of tens of nanometers, they speculated that mass transport primarily occurs in the macroporous domain, which should play a key role in permeability. Regarding pore size distribution in the catalyst layer, their analysis showed that the majority of pores were smaller than 200 nm. This finding is relevant to capillarity, where larger pores facilitate dominant gas removal, while smaller pores with higher capillary pressures serve as key pathways for liquid transport. The nanoCT results finally enabled the authors to examine the dispersion of Ir particles as agglomerates. As the distribution of Ir affects the electrical and protonic conductivities of PEMWEs,[61] they used network modeling to determine transport properties. In this case, optimizing agglomerate sizes was proposed to enhance conductivity and increase catalyst utilization, as also suggested by Leonard et al.[32]

Following a similar approach in evaluating catalyst layers using TXM, Zhao et al.[34] expanded the existing knowledge to enhance PEMWE performance by directly targeting the engineering of IrO_x-ionomer agglomerates and IrO_x aggregate structures. The authors introduced interconnected submicron pores and nanocavities within these structures to optimize mass transport. This approach addressed the issue in the above studies, in which efforts to improve mass transport within the catalyst layer overlooked the densely packed agglomerates that decrease useful surface area for the OER. By using octadecanethiol as a templating agent, the "packaging" of agglomerates was tuned. This templating method was used to increase spacing among IrO_x particles, enhancing bubble nucleation and reducing diffusion resistance, thereby improving transport through the catalyst layer. Using nanoCT, the authors observed a shift in pore size distribution from a conventional catalyst layer to a templated one, detecting a greater number of small pores (~60 nm)

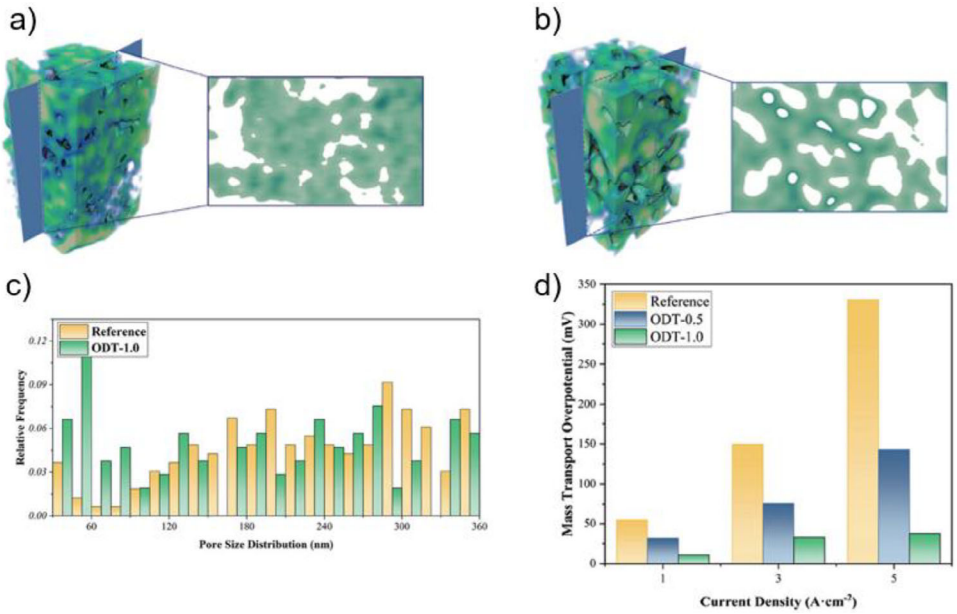

Figure 10. 3D reconstruction images and 2D slices for a) the conventional anode CL and b) modified with octadecanethiol-1.0 CL. c) Pore structure analysis results derived from the 3D reconstruction images for octadecanethiol-1.0 and the conventional anode CL. d) Recorded electrolysis performance and the corresponding mass transport overpotential deconvolution result for octadecanethiol-0.5, octadecanethiol-1.0, and the conventional MEA with the anode CL. Reprinted from Ref. [34] and used under the Creative Commons License (CC BY 4.0.).

(Figure 10). It was also demonstrated that the modified catalysts had improved catalyst utilization and reduced transport overpotentials.

The above studies indicate that nanoCT is a unique tool for in-depth characterization of the CL, offering superior resolution compared to microCT or conventional radiography. When analyzing agglomerates, assessing their 3D dispersion, or identifying pores and channels, the quality and representativeness of data are crucial for further analysis and precise identification of voids and catalyst space occupancy. In this case, nanoCT provides high-quality 3D data while also preserving the sample, unlike FIB-SEM, and can also be less time-consuming, making it possible for dataset screening. However, despite being a nondestructive technique, sample preparation remains an important consideration, as nanoCT requires for the measurement of smaller volumes compared to microCT, necessitating a compromise on representativeness as discussed earlier in this section. Further improvements of the technique will allow faster data acquisition,[63,64] making it possible to evaluate more samples or larger regions of interest. Finally, it is noteworthy to highlight that, to the best of the authors' knowledge, so far only CLs have been investigated by nanoCT. This provides space for further discussions on different layers or interfaces, such as PTLs or PTEs, where the assembly of the catalyst layer may also interact with the transport layer content.

2.5. Chemical Imaging with Synchrotron-Based X-Ray Microscopy

The studies in Section 2.4 dealing with PEMWE cell structure and morphology have primarily used microCT, nanoCT, or radiography for spatially and temporally resolved analysis based on direct imaging. However, the local chemical structure of PEMWE systems can also be investigated by combining tomography or microscopy with complementary techniques based on various interactions of X-rays. This approach is known as chemical imaging. In comparison to the direct imaging studies shown previously, comparatively fewer groups have explored the potential of synchrotron-based X-rays for spatially-resolved chemical imaging.[11] Acquisition modes such as absorption, diffraction, and fluorescence can be effectively used to map PEMWE structures in 2D or 3D. Applications include studying catalyst layer degradation and identifying different phases within the MEA structure. Additionally, ex situ, in situ, or *operando* analyses are feasible if the necessary hardware is available—meaning access to appropriate beamlines with sufficient resolution and acquisition methods, combined with suitable test cells to address chemical characterization challenges. It should be noted that while direct imaging via microCT, nanoCT, or radiography is in principle possible in dedicated laboratory instruments, most chemical imaging methods depend on synchrotron radiation to achieve adequate results, as outlined in the following examples.

Among the few studies using synchrotron X-rays for chemical mapping of PEMWE, the work of Zaccarine et al.[21] combined 2D TXM with XANES. This specific combination can access information about local structure (e.g., oxidation state) and coordination environment of the specific element of interest. During *operando* XAS studies of PEMWE electrocatalysts, the coexistence of different Ir oxidation states was observed even at high anodic potentials, along with surface changes linked to varying OER mechanisms.[65,66] Therefore, 2D TXM with XANES was applied ex situ to investigate catalyst layer degradation under steady-state and intermittent operation regimes. In this study, the authors

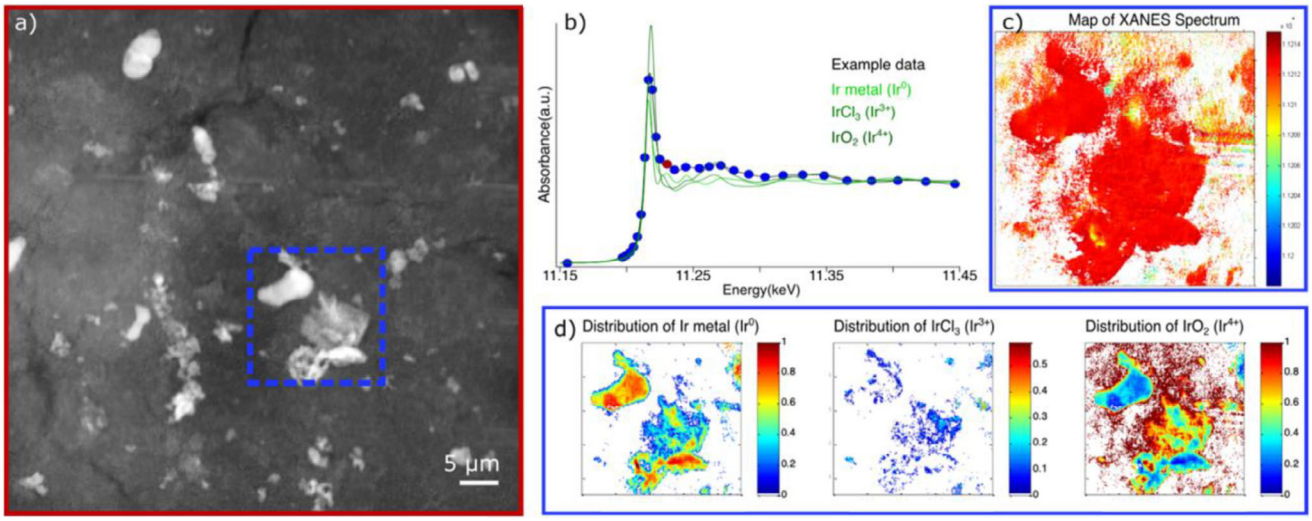

Figure 11. Schematic of information that can be obtained from TXM analysis. (a) Example TXM 4 × 4 mosaic image comprised of 16 image tiles for a wider FOV image. (b) XANES spectral overlay of example data from a sample (black), the Ir metal reference (light green), $IrCl_3$ reference (green), and IrO_2 reference (dark green). The blue circles represent data points collected at multiple energies along the absorption edge, and the red circle represents the location where an image and/or spectrum can be collected "above the edge." (c) Example chemical map obtained by collecting an image at points along the entire XANES spectrum (blue circles in b) for the sample from the region indicated by the blue box in a. The color gradient represents the energy of the edge jump (the energy at which the intensity is halfway between the pre- and post-edge linear fits). (d) Example distribution of each standard species in the same region as the chemical map. Here, the gradient is based on total % of the sample's composition, since the normalization function normalized by thickness, such that each pixel adds up to 100% by summing the different Ir species included in their fit. Reprinted from Ref. [21] and used under the Creative Commons License (CC BY 4.0.).

used a CCM, Toray paper as PTL (anodic and cathodic), and Ir or IrO_2 as the anode catalyst for the MEA. After electrocatalytic testing, ex situ imaging was performed on sections of the CCM cut from the center of the original sample. The experiment achieved a pixel size of 23 nm, while XANES analysis was conducted with energy variations from 11.145 to 11.472 keV over the Ir L_3 edge. Due to resolution limitations, only larger agglomerates of Ir and IrO_2 were resolved as shown in Figure 11. This limited the visualization of the ionomer, which exhibited lower absorption contrast. Their results showed a distinct distribution of Ir^0, Ir^{3+}, and Ir^{4+} in different samples (fresh and tested catalysts) through XANES-TXM characterization. Additionally, catalysts based on Ir black were found to be less stable than IrO_2-based catalysts, as demonstrated by the dispersion of Ir species throughout the catalyst layer after being subjected to a 2 V voltage hold in both cases, indicating detachment from agglomerates or aggregates. Based on these findings, the authors concluded that XANES-TXM is an excellent technique for mapping and differentiating species while identifying various oxidation states within PEMWE. This technique is particularly useful for defining chemical degradation mechanisms and understanding their spatial distribution of different oxidation states for a variety of elements. However, it is important to mention that for ex situ experiments Ir species can oxidize during handling outside the electrochemical cell, leading to probable differences in the results compared to hypothetical in situ studies. Therefore, designing a cell that allows TXM 2D imaging and XANES in situ could represent a next step toward this type of analysis.

Following a broader approach than Zaccarine et al.[21] in 2D mapping of PEMWE, a previous study by the authors of this article (Rex et al.[20]) applied 2D XRF to evaluate metal migration through MEAs with a CCM configuration. This approach captured CLs and solid electrolyte on a larger scale as an alternative method to study degradation and how it affects, directly or indirectly, the entire membrane structure. In this case, the membranes were tested in a Fraunhofer ISE cell with an active area of 4 cm^2 under different stressing conditions (operation time and impurities added to the water flow). The chosen voltage for the experiments was constant at 2 V. A large area of the parent membranes (4 cm^2) was measured after preparing sample slices with a microtome. Analysis was performed across these CCM slices with a FOV of approximately 200 × 75 µm, generating 2D maps of Pt, Ir, Fe, and Ti. The synchrotron experiment (SLS) was carried out at different energies (11.0, 11.4, and 11.7 keV), with a 1 µm beam size that generated emission signals for each pixel of the map. The datasets were later fit to identify the elements present in both the catalyst layers and Nafion membrane. These results showed that Ir and Pt migrated intensively toward the Nafion membrane, but with different diffusion behaviors depending on the stress test conditions, as shown for Ir migration in Figure 12. A model contamination source (water contaminated with Fe^{2+}) also influenced the metal migration, causing different migration behavior compared to the samples stressed without contaminants.

This study revealed the importance of evaluating the region within the Nafion membrane and catalyst layer, highlighting that more degradation mechanisms are probably present than previously understood. XRF mapping proved to be effective in resolving metal migration within the membrane through a high-throughput analysis (40 min to 2 h depending on sample size), with a relatively large FOV when compared to electron microscopy techniques. However, while the technique provided

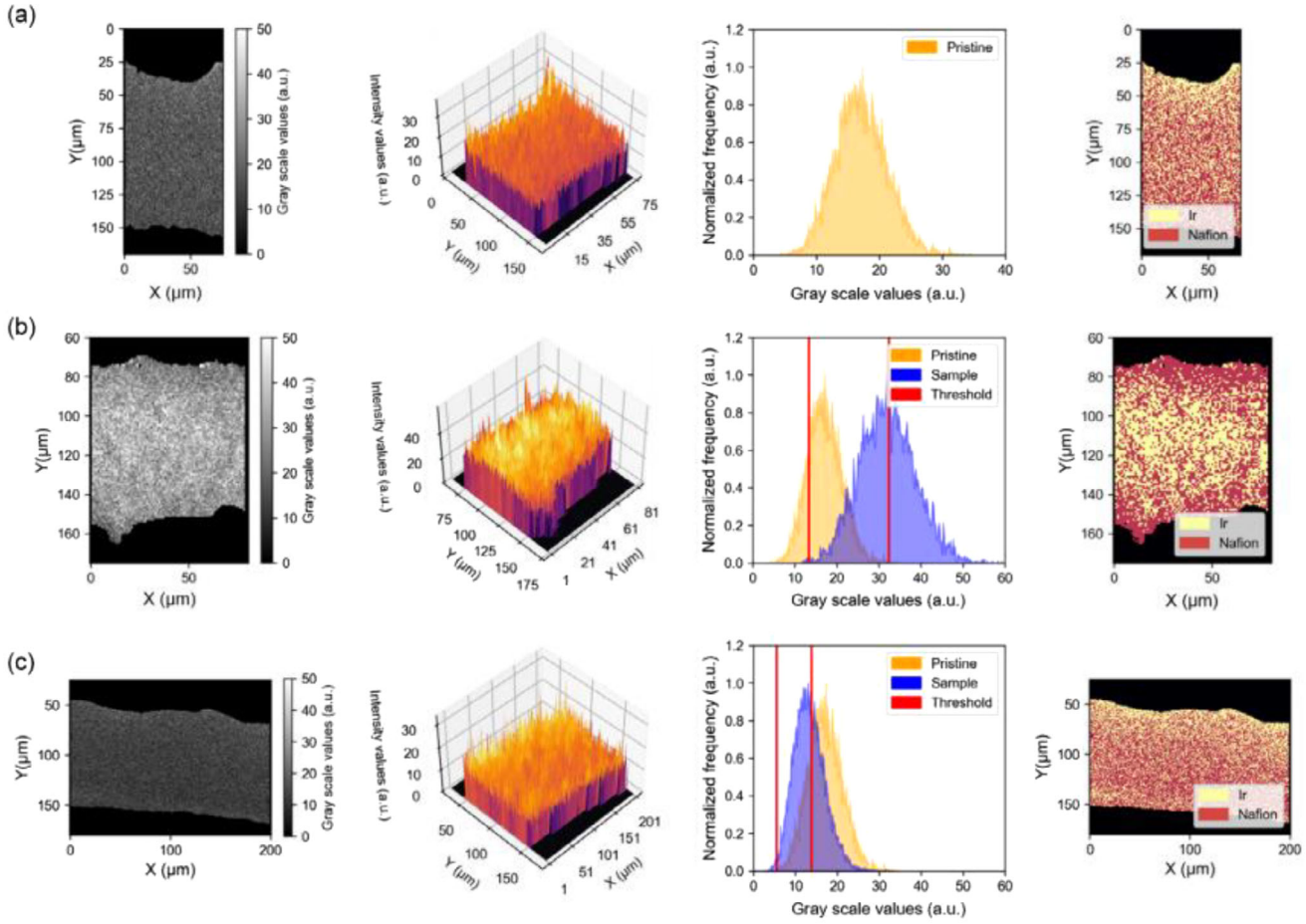

Figure 12. Ir XRF emission signal (beam energy of 11.7 keV) for multiple samples using Pristine CCM as reference. Segmented Nafion region and corresponding histograms followed by the elemental map: a) Ir XRF emission signal – Pristine CCM III, b) Ir XRF emission signal – 100 h CV CCM, and c) Ir XRF emission signal – Fe^{2+}-contaminated CCM. Reprinted from Ref. [20] and used under the Creative Commons License (CC BY 4.0.).

accurate chemical maps, we also suggest improvements, such as performing in situ evaluation or increasing resolution at the expense of analysis time, to better assess elemental profiles at the catalyst layer/Nafion membrane interface. It is important to note that traditional techniques such as SEM-EDX or lab-XRF may not be sensitive enough to visualize the samples in this way, as apparent from the lack of literature reports on this topic, therefore demonstrating the unique advantage of synchrotron XRF mapping in this context.

Following the 2D imaging studies for acquiring chemically relevant information, important measurements were performed in 3D using ptychographic X-ray computed tomography (PXCT) by De Angelis et al.[35] PXCT is a high-resolution nanoscale tomography method which is only feasible at synchrotron light sources due to the need for coherent hard X-rays. When using ptychography, overlapping diffraction patterns are measured using a coherent X-ray beam and reconstructed with phase retrieval algorithms. This produces high resolution nanoscale images of the sample, allowing a clear separation of features such as porosity and different solid components[67] within the PEMWE catalyst layer. Notably, PXCT is a phase-contrast microscopy method which does not depend on sample crystallinity or state of matter, only on the local electron density of the sample. So far, many studies have presented reconstructions of the PTL, as mentioned earlier in this work. However, to the best of our knowledge, very few studies presented the complete reconstruction of the CL with 3D spatially-resolved imaging, and even fewer successfully reconstructed the ionomer structure.[68] As a result, previous works have relied on simulations to better understand the behavior of these critical components of the PEMWE, as shown by Bazylak et al.[33,69]

For the first time, to the best of the authors knowledge, De Angelis et al.[35] successfully resolved the ionomer layer in IrO_2/TiO_2 CL using PXCT by achieving sufficient contrast between different oxides phases within the catalyst, ionomer, and pores, allowing image segmentation of each component within the sample. In their experiment, a cross-section of the catalyst layer was extracted using FIB-SEM, then evaluated under vacuum and cryogenic conditions at the cSAXS beamline (SLS) to ensure the stability of the ionomer phase against beam damage. The experiment provided a pixel size of 16 nm resulting in phase distribution that was captured in a 5×5 µm region of interest (see Figure 13), demonstrating the power of PXCT in separating the ionomer phase from other parts of the catalyst layer with a clear distribution and 3D spatial resolution. From this separation, the technique identified all expected components (TiO_2,

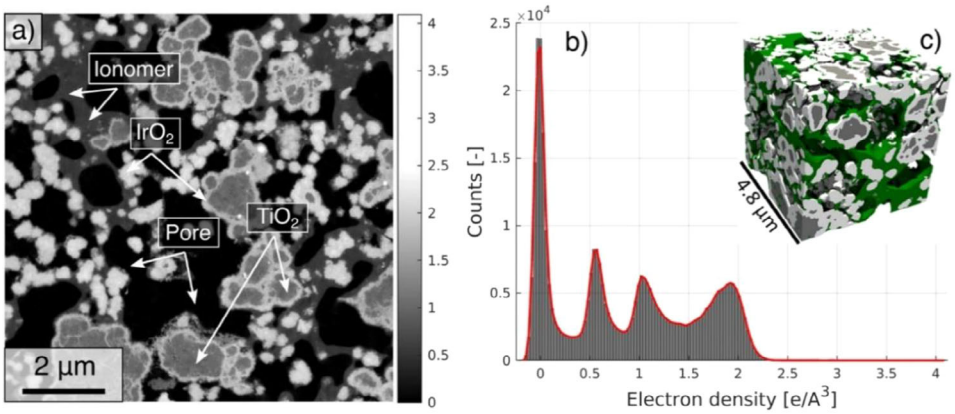

Figure 13. (a) 2D slice obtained from the entire tomogram showing all phases present in the electrode. In (a), the grayscale values represent the electron density expressed in e/A^3. (b) Electron density histogram calculated over the entire volume. (c) 3D rendering of a subvolume extracted from the full segmented dataset. In (c), the white phase is the —IrO_2, the gray phase is the —TiO_2, and the green phase is the ionomer and the porosity transparent. Reprinted from Ref. [35] and used under the Creative Commons License (CC BY 4.0.).

IrO_2, ionomer, and pores), revealing a core-shell structure for IrO_2/TiO_2, confirming TiO_2 in its rutile form, and showing that IrO_2 exhibits a lower-than-expected electron density, possibly due to nanoporosity beyond the spatial resolution limit. Furthermore, important aspects such as ionomer distribution (which interconnects agglomerates but does not coat IrO_2 uniformly) were discussed, and later indicating that ionic conductivity is the limiting factor in the nonswollen ionomer structure. Overall, the study highlighted PXCT as a powerful tool for simultaneously characterizing the structures of different phases within PEMWE CL in a noninvasive manner.

Furthermore, Weber et al.[36] expanded their ptychography study using synchrotron-based ptychographic X-ray laminography (PyXL). This technique combines ptychography with laminography to enable high-resolution 3D imaging of thin and extended samples, while rotation occurs by tilting the sample at an angle (typically off-axis) and rotating it on vertical axis during X-ray exposure.[70] This allows for larger lateral fields of view, therefore potentially improving the representativeness of the measurement. The novelty in their work was the evaluation of PEMWE under dry and wet conditions. Weber et al.[36] compared CCM and PTE components with three different loadings (close to the required targets of 0.05 g_{Ir}/kW),[12,71,72] while using an MPL layer to improve diffusion conditions. Finally a thin Pt protective layer was introduced on the MPL to create a complex multilayered system. Since evaluating such a layer is a multiscale challenge, PyXL was chosen for catalyst layer evaluation at micrometer scale because it allows larger samples (planar) to be mounted. Their results with PyXL notably reached a voxel size of 35 nm for a region of 20×20 µm x CL thickness, presenting minor differences in contrast compared to previous PXCT results by the same group[35] (due to cryogenic conditions in the former experiment). A similar core-shell structure of IrO_2/TiO_2 and the film formed by the ionomer was also revealed, which acts as a binder and creates a network for the aggregates and agglomerates (Figure 14). Unfortunately, due to the lower contrast after flooding the samples with water, the ionomer phase could not be segmented under wet conditioning, allowing to only investigate the solid phases (IrO_2 and TiO_2) of the system. Moreover, only the particle diameters of IrO_2 and TiO_2 in dry and wet states through phase differentiation could be compared, concluding similar profiles for volume fraction versus particle diameter.

From PyXL, it is important to highlight that this technique could allow future measurement of PEMWE samples without the need for FIB-SEM to retrieve a part of the catalyst layer. This would save time and avoid sample destruction during preparation, leading to further insights for 3D characterization in situ or *operando* due to the geometric configuration of such experiments.[73]

As a general guideline related to chemical characterization by the means of synchrotron-based, spatially-resolved techniques, it is extremely important to notice a compromise related to the experiment time, imaged ROI, and spatial resolution,[18] in which two of these parameters are normally prioritized at the expense of the third. Currently, many synchrotrons around the world are upgrading to 4th generation, leading to improved coherence properties which can improve experiments such as PXCT and PyXL both with respect to measurement time and resolution. Finally, regarding multiacquisition modes, it is also considered that for each technique an expertise is necessary, from experimental tasks to data processing, providing opportunities for intelligent models to process and interpret large and complex data volumes generated by tomography.[74,75]

2.6. Further Aspects on Synchrotron X-ray Imaging (Image Acquisition, Computational Methods, and Application)

The case studies in this review represent the great potential of spatially- and chemically-resolved imaging techniques in disentangling, at different scales, the interplay between structural and transport-related parameters with the lifetime and performance of PEMWE. Despite these advances, cutting edge techniques such as X-ray laminography or 2D XRF mapping are not yet routinely performed in the domain of water electrolyzers. In

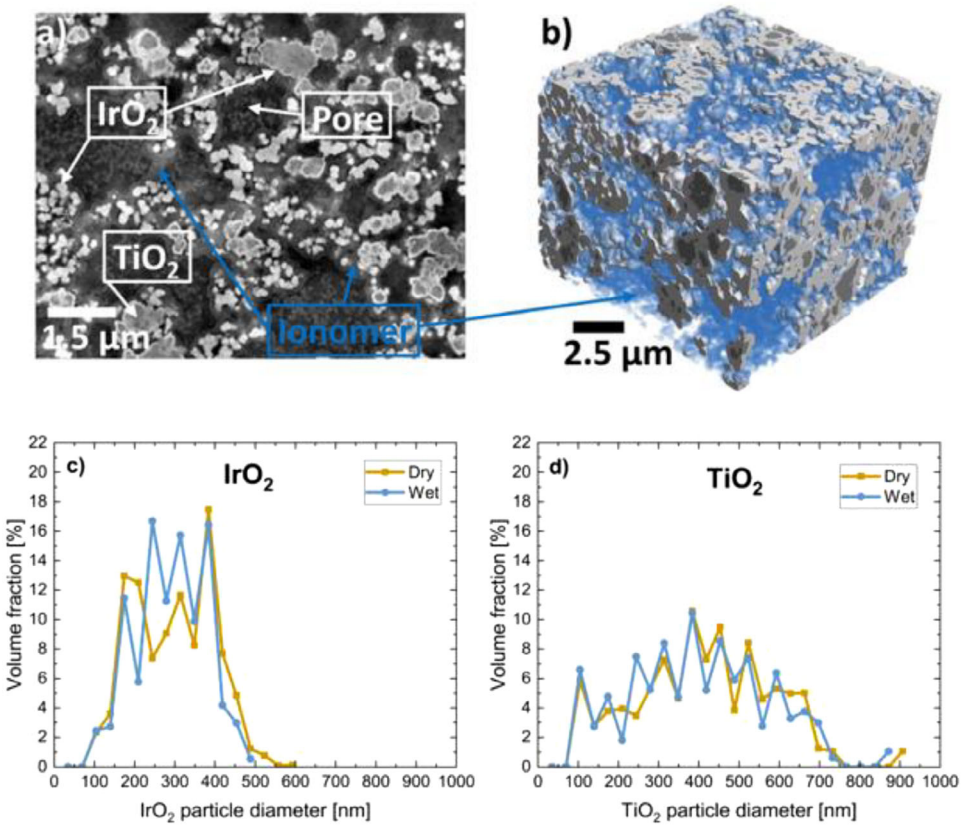

Figure 14. (a) Grey-scale slice of the CL (dry) extracted from the 3D volume obtained by PyXL, (b) surface rendering of the volume with the ionomer phase shown in blue (c) IrO_2 particle diameter, and (d) TiO_2 particle diameter. For (c) and (d) the data for the wet CL are included. Adapted from Ref. [36] with permission from the Royal Society of Chemistry.

this section, we discuss what can be improved to strengthen the complementarity between standard electrochemical performance, X-ray imaging techniques, and advanced synchrotron characterization.

2.6.1. Image Acquisition and Cell Design

Performing in situ and *operando* imaging in complex systems such as PEMWE is challenging because technical modifications to the standard PEMWE designs are usually required to ensure good signal quality and/or the possibility to probe ROIs large enough to represent the phenomena of interest. These modifications may consist of using gasket and bipolar plates which are transparent to X-rays, in using home-made cells, in the partial or total disassembly of the PEM cell, or in drilling channels and holes to ensure the X-ray pathway to and from the investigated ROIs. The trade-off in these approaches is that by improving the possibility of performing spatially-resolved analysis, this introduces deviation from the standard PEM designs, which can lead to local or global variations in parameters and experimental conditions. For instance, a design optimized for radiation pathways through the cell is usually thinner in at least one spatial dimension to reduce beam attenuation. However, this can negatively affect transport processes related to bubble removal. Moreover, a modification intended to image a specific component may not be suitable for simultaneously probing other parts of the electrolyzer at a technical scale. For this reason, there are no standardized PEM cell designs for in situ/*operando* X-ray imaging investigations. Other research groups not directly involved in X-ray imaging are also addressing this challenge. Recent studies focused on cell design for synchrotron-based spectroscopies—such as X-ray absorption spectroscopy and small-angle X-ray scattering—can serve as starting points for further modifications related to MEA thickness, light path optimization, and bubble management.[76,77] These technical and practical gaps can potentially be minimized by combining new in situ/*operando* cell designs which are optimized for tomography measurements, and which allow data recovery noninvasively. Implementing advanced image processing algorithms can help even more in minimizing the invasiveness of PEM design modification, with an additional gain also on the temporal resolution for *operando* characterization: For instance, sparse imaging methods have previously been used to overcome the challenge of using a wide tilting angle[78] in ptychography experiments or to avoid using high radiation doses on sensitive samples.[79] These protocols are used together with machine learning algorithms to expand dimensionality or to reconstruct and predict missing information from sparse tomography,[63,80] making them very suitable to be applied to sensitive Nafion membranes without invasive PEM modifications.

2.6.2. Data Reusability and Computational Methods

As pointed out by Finegan et al.,[81] there are usually systematic limitations in terms of sample preparation or technical limitations for each technique that prevent the acquisition of multimodal and multiscale details from the same sample. This makes the necessity for routine *operando* X-ray-based imaging applied to PEMWE even more compelling in order to have datasets that are diverse and large enough to apply machine learning algorithms capable of 1) accelerating image processing routines such as segmentation and artifact corrections, which can be very time-consuming for large volumes of images, and 2) correlating information from different scales and performing optimization which takes into account the mutual influence of the individual components of PEMWE. This concept and integrated framework are already employed in battery research,[81,82] while it is still missing in the water electrolyzer research community or limited to the optimization of single components.,[83] This is mostly because of the presence of liquid and gaseous phases which increase the difficulty in performing in situ and *operando* imaging, as stated in the previous sections. Computer vision algorithms to speed up image processing and correlative integrated frameworks both require high quality, standardized image datasets, which can be reached faster as more and more researchers explore spatial and chemically resolved X-ray techniques. An effective combination of multiscale imaging techniques, modelling and machine learning algorithms, would be a powerful tool to correlate structural features with mass transfer and/or kinetic limitations, as well as in optimization of PEMWE cell designs, both for standardized complementary characterization and for industrial devices.[84]

3. Summary and Outlook

PEMWE systems are complex technical devices with hierarchical structures, so it is crucial that many different evaluation techniques are available to better understand and improve the function of such devices. When extending from model systems toward device-like or even technical/industrial systems, it becomes increasingly challenging to bridge the gap and obtain meaningful characterization data on representative samples. As discussed throughout this article, different case studies can be addressed by the use of synchrotron-based techniques, creating opportunities for future researchers to optimize and improve the industrial viability of PEMWE designs. The design, structure, and composition of such devices are crucial when aiming to reduce Ir loading or increasing their lifetime, for example. As shown here, radiography, microCT, nanoCT, and other techniques, when used together, play a significant role in understanding degradation mechanisms, the association of different components within PEMWE, and also in elucidating synthesis aspects by tuning various parameters that can affect local composition and structure.

Currently, an important research direction is to focus on more realistic case studies in order to understand real behavior during operation, as it was done by Leonard et al.[32] and later by De Angelis et al.[28] when using Ti PTLs in X-ray imaging experiments. In both cases, spatially- and time-resolved profiling led to important results that later changed the evaluation benchmark. Although such achievements are already impressive, further characterization is needed to better understand the phenomena related to chemical gradients, such as how Ir species behave within the PTL or Nafion membrane, as demonstrated by radiography and XRF mapping, respectively. It is also clear that such systems are geometrically challenging to assemble on a beamline while measuring *operando* or in situ. However, conducting research to achieve different configurations or designing new cells for future measurements is now seen as essential to investigate the numerous phenomena that may contribute to degradation (either physically or chemically), or to understand fundamental parameters that can improve operation (water flow, current, materials used to build MEAs, etc.). Although assembling and testing new PEM cell designs is time consuming, the increasing availability of laboratory X-ray instruments suitable for fluorescence mapping and/or absorption spectroscopy can accelerate the routine investigation based on in situ imaging and spectroscopy at least at the microscale. Furthermore, such insights could later be better processed and used for simulations, saving an enormous amount of time in research focused on optimization through extensive sample screening.

This article aims to clarify how the use of synchrotron-based hard X-rays can benefit the field of technical electrochemistry by providing spatially-resolved, and in some cases time-resolved data on device-like systems. It is also relevant that given the relatively few groups currently operating in this space, the full potential of such techniques has not yet been reached. As the accessibility and characterization potential of modern synchrotron light sources is continually evolving and improving, the timing is appropriate to highlight the novel research performed at such facilities, and to inspire other users to consider hard X-ray imaging methods as part of the modern characterization toolkit. Such methods can readily complement established laboratory characterization, and in some cases multiple X-ray analytics can be combined to provide additional information. Although the state of the art as indicated here commonly involves individual X-ray imaging studies in isolation, multimodal approaches represent an important direction for future electrolysis research. Together with sophisticated methods as well as classic characterization and benchmarking, a comprehensive understanding on the operation and durability of PEMWE devices is feasible, leading to conclusions about a very broad and multiscaled technical system while bridging the gap between academia and industry.

Acknowledgments

L.A.C. and T.L.S. acknowledge financial support from the German Federal Ministry of Research, Technology and Space (BMFTR) Röntgen-Ångstrom Cluster (RÅC) project 13K22VKA. J.S. acknowledges financial support from the Carl-Zeiss-Stiftung. The authors acknowledge TU Wien Bibliothek for financial support through its Open Access Funding Programme.

Conflict of Interests

The authors declare no conflict of interest.

Keywords: Characterization · Electrolysis · PEMWE · Synchrotron radiation · Tomography

[1] G. Luderer, S. Madeddu, L. Merfort, F. Ueckerdt, M. Pehl, R. Pietzcker, M. Rottoli, F. Schreyer, N. Bauer, L. Baumstark, C. Bertram, A. Dirnaichner, F. Humpenöder, A. Levesque, A. Popp, R. Rodrigues, J. Strefler, E. Kriegler, *Nat. Energy*, **2022**, *7*, 32–42.
[2] A. Makhsoos, M. Kandidayeni, B. G. Pollet, L. Boulon, *Int. J. Hydrogen Energy* **2023**, *48*, 15341–15370.
[3] C. Van Pham, D. Escalera-López, K. Mayrhofer, S. Cherevko, S. Thiele, *Adv. Energy Mater.* **2021**, *11*, 2101998.
[4] Y. Wang, Y. Pang, H. Xu, A. Martinez, K. S. Chen, *Energy Environ. Sci.* **2022**, *15*, 2288–2328.
[5] H. Miyaoka, T. Ichikawa, Y. Kojima, *Int. J. Hydrogen Energy* **2018**, *43*, 14486–14492.
[6] A. Kowalski, G. Faber, E. Cave, *Curr Opin Green Sustain Chem* **2023**, *39*, 100702.
[7] H. B. Tao, H. Liu, K. Lao, Y. Pan, Y. Tao, L. Wen, N. Zheng, *Nat. Nanotechnol.* **2024**, *19*, 1074–1076.
[8] M. Milosevic, T. Böhm, A. Körner, M. Bierling, L. Winkelmann, K. Ehelebe, A. Hutzler, M. Suermann, S. Thiele, S. Cherevko, *ACS Energy Lett.* **2023**, *8*, 2682–2688.
[9] S. A. Grigoriev, D. G. Bessarabov, V. N. Fateev, *Russ. J. Electrochem.* **2017**, *53*, 318–323.
[10] H. Yu, L. Bonville, J. Jankovic, R. Maric, *Appl. Catal. B* **2020**, *260*, 118194.
[11] Y. Chen, G. Stelmacovich, A. Mularczyk, D. Parkinson, S. K. Babu, A. Forner-Cuenca, S. Pylypenko, I. V. Zenyuk, *ACS Catal.* **2023**, *13*, 10010–10025.
[12] C. Minke, M. Suermann, B. Bensmann, R. Hanke-Rauschenbach, *Int. J. Hydrogen Energy* **2021**, *46*, 23581–23590.
[13] A. Buttler, H. Spliethoff, *Renewable Sustainable Energy Rev.* **2018**, *82*, 2440–2454.
[14] A. Beck, M. Zabilskiy, M. A. Newton, O. Safonova, M. G. Willinger, J. A. van Bokhoven, *Nat. Catal.* **2021**, *4*, 488–497.
[15] J. Schröder, V. A. Mints, A. Bornet, E. Berner, M. Fathi Tovini, J. Quinson, G. K. H. Wiberg, F. Bizzotto, H. A. El-Sayed, M. Arenz, *JACS Au* **2021**, *1*, 247–251.
[16] M. A. Bañares, *Catal. Today* **2005**, *100*, 71–77.
[17] A. Prajapati, C. Hahn, I. M. Weidinger, Y. Shi, Y. Lee, A. N. Alexandrova, D. Thompson, S. R. Bare, S. Chen, S. Yan, N. Kornienko, *Nat. Commun.* **2025**, *16*, 1–20.
[18] S. Das, R. Pashminehazar, S. Sharma, S. Weber, T. L. Sheppard, *Chem. Ing. Tech.* **2022**, *94*, 1591–1610.
[19] J. D. Grunwaldt, C. G. Schroer, *Chem. Soc. Rev.* **2010**, *39*, 4741.
[20] A. Rex, L. Almeida De Campos, T. Gottschalk, D. F. Sanchez, P. Trinke, S. Czioska, E. Saraçi, B. Bensmann, J. D. Grunwaldt, R. Hanke-Rauschenbach, T. L. Sheppard, *Adv. Energy Sustainability Res.* **2024**, *5*, 2400048.
[21] S. F. Zaccarine, S. Meital, J. N. Weker, M. J. Dzara, J. Foster, M. Carmo, S. Pylypenko, *J. Electrochem. Soc.* **2022**, *169*, 064502.
[22] G. Stelmacovich, S. Pylypenko, *ChemElectroChem* **2024**, *11*, e202400377.
[23] M. C. Yasin, M. Johar, A. Gupta, S. Shahgaldi, *Int. J. Hydrogen Energy* **2024**, *88*, 726–747.
[24] W. Xia, J. Zhang, G. Xu, T. Jin, Q. Wang, L. Jiao, *Next Materials* **2025**, *8*, 100553.
[25] J. T. Lang, D. Kulkarni, C. W. Foster, Y. Huang, M. A. Sepe, S. Shimpalee, D. Y. Parkinson, I. V. Zenyuk, *Chem. Rev.* **2023**, *123*, 9880–9914.
[26] I. V. Zenyuk, *Curr. Opin. Electrochem.* **2019**, *13*, 78–85.
[27] E. Leonard, A. D. Shum, S. Normile, D. C. Sabarirajan, D. G. Yared, X. Xiao, I. V. Zenyuk, *Electrochim. Acta* **2018**, *276*, 424–433.
[28] S. De Angelis, T. Schuler, M. A. Charalambous, F. Marone, T. J. Schmidt, F. N. Büchi, *J. Mater. Chem. A Mater.* **2021**, *9*, 22102–22113.
[29] X. Peng, P. Satjaritanun, Z. Taie, L. Wiles, A. Keane, C. Capuano, I. V. Zenyuk, N. Danilovic, *Adv. Sci.* **2021**, *8*, e2102950.
[30] D. Kulkarni, A. Huynh, P. Satjaritanun, M. O'Brien, S. Shimpalee, D. Parkinson, P. Shevchenko, F. DeCarlo, N. Danilovic, K. E. Ayers, C. Capuano, I. V. Zenyuk, *Appl. Catal. B* **2022**, *308*, 121213.
[31] D. Kulkarni, R. Ouimet, B. Erb, D. Y. Parkinson, H. M. Chang, C. Wang, A. Smeltz, C. Capuano, I. V. Zenyuk, *ACS Appl. Mater. Interfaces* **2023**, *15*, 48060–48071.
[32] E. Leonard, A. D. Shum, N. Danilovic, C. Capuano, K. E. Ayers, L. M. Pant, A. Z. Weber, X. Xiao, D. Y. Parkinson, I. V. Zenyuk, *Sustain. Energy Fuels* **2020**, *4*, 921–931.
[33] J. K. Lee, P. Kim, K. Krause, P. Shrestha, M. Balakrishnan, K. Fahy, K. Fatih, N. Shaigan, M. Ge, W. K. Lee, A. Bazylak, *Cell Rep. Phys. Sci.* **2023**, *4*, 101232.
[34] C. Zhao, S. Yuan, X. Cheng, S. Shen, N. Zhan, R. Wu, X. Mei, Q. Wang, L. An, X. Yan, J. Zhang, *Adv. Energy Mater.* **2024**, *14*, 2401588 https://doi.org/10.1002/aenm.202401588.
[35] S. De Angelis, T. Schuler, M. Sabharwal, M. Holler, M. Guizar-Sicairos, E. Müller, F. N. Büchi, *Sci. Rep.* **2023**, *13*, 4280.
[36] C. C. Weber, S. De Angelis, R. Meinert, C. Appel, M. Holler, M. Guizar-Sicairos, L. Gubler, F. N. Büchi, *EES Catalysis* **2024**, *2*, 585–602.
[37] M. Bierling, D. McLaughlin, B. Mayerhöfer, S. Thiele, *Adv. Energy Mater.* **2023** *13*, 2203636.
[38] J. K. Lee, G. Anderson, A. W. Tricker, F. Babbe, A. Madan, D. A. Cullen, J. D. Arregui-Mena, N. Danilovic, R. Mukundan, A. Z. Weber, X. Peng, *Nat. Commun.* **2023**, *14*, 4592.
[39] M. Bühler, P. Holzapfel, D. McLaughlin, S. Thiele, *J. Electrochem. Soc.* **2019**, *166*, F1070–F1078.
[40] R. T. Liu, Z. L. Xu, F. M. Li, F. Y. Chen, J. Y. Yu, Y. Yan, Y. Chen, B. Y. Xia, *Chem. Soc. Rev.* **2023**, *52*, 5652–5683.
[41] N. Sezer, S. Bayhan, U. Fesli, A. Sanfilippo, *Mater. Sci. Energy Technol.* **2025**, *8*, 44–65.
[42] D. Zhang, Z. Wang, K. Huang, *Int. J. Hydrogen Energy* **2013**, *38*, 11379–11391.
[43] M. Prestat, *J. Power Sources* **2023**, *556*, 232469.
[44] J. T. Mefford, A. R. Akbashev, M. Kang, C. L. Bentley, W. E. Gent, H. D. Deng, D. H. Alsem, Y. S. Yu, N. J. Salmon, D. A. Shapiro, P. R. Unwin, W. C. Chueh, *Nature* **2021**, *593*, 67–73.
[45] A. R. Akbashev, V. Roddatis, C. Baeumer, T. Liu, J. T. Mefford, W. C. Chueh, *Energy Environ. Sci.* **2023**, *16*, 513–522.
[46] T. Kosmala, A. Baby, M. Lunardon, D. Perilli, H. Liu, C. Durante, C. Di Valentin, S. Agnoli, G. Granozzi, *Nat. Catal.* **2021**, *4*, 850–859.
[47] S. J. Altus, B. J. Inkson, J. Hack, *J Mater. Chem. A Mater.* **2024**, *12*, 23364–23391.
[48] J. Liu, E. Medici, A. T. Haug, D. A. Cullen, K. Tajiri, J. S. Allen, I. V. Zenyuk, *Int. J. Hydrogen Energy* **2022**, *47*, 17749–17761.
[49] K. J. Ferner, J. Park, Z. Kang, S. A. Mauger, M. Ulsh, G. Bender, S. Litster, *Int. J. Hydrogen Energy* **2024**, *59*, 176–186.
[50] F. Hegge, R. Moroni, P. Trinke, B. Bensmann, R. Hanke-Rauschenbach, S. Thiele, S. Vierrath, *J. Power Sources* **2018**, *393*, 62–66.
[51] S. Xu, H. Liu, N. Zheng, H. B. Tao, *Adv. Mater. Interfaces* **2025**, *12*, 2400549.
[52] T. Kadyk, D. Bruce, M. Eikerling, *Sci. Rep.* **2016**, *6*, 1–14.
[53] Z. Lu, L. Zhang, R. Iwata, E. N. Wang, J. C. Grossman, *Langmuir* **2020**, *36*, 15112–15118.
[54] S. Yuan, C. Zhao, X. Cai, L. An, S. Shen, X. Yan, J. Zhang, *Prog. Energy Combust. Sci.* **2023**, *96*, 101075.
[55] A. Bazarah, E. H. Majlan, T. Husaini, A. M. Zainoodin, I. Alshami, J. Goh, M. S. Masdar, *Int. J. Hydrogen Energy* **2022**, *47*, 35976–35989.
[56] L. Salvo, P. Cloetens, E. Maire, S. Zabler, J. J. Blandin, J. Y. Buffière, W. Ludwig, E. Boller, D. Bellet, C. Josserond, *Nucl. Instrum. Methods Phys. Res. B* **2003**, *200*, 273–286.
[57] F. García-Moreno, T. R. Neu, P. H. Kamm, J. Banhart, *Adv. Eng. Mater.* **2023**, *25*, 2201355.
[58] Z. Taie, X. Peng, D. Kulkarni, I. V. Zenyuk, A. Z. Weber, C. Hagen, N. Danilovic, *ACS Appl. Mater. Interfaces* **2020**, *12*, 52701–52712.
[59] T. Schuler, J. M. Ciccone, B. Krentscher, F. Marone, C. Peter, T. J. Schmidt, F. N. Büchi, *Adv. Energy Mater.* **2020**, *10*, 1903216.
[60] E. Maire, P. J. Withers, *International Materials Reviews* **2014**, *59*, 1–43.
[61] M. Inaba, A. Zana, J. Quinson, F. Bizzotto, C. Dosche, A. Dworzak, M. Oezaslan, S. B. Simonsen, L. T. Kuhn, M. Arenz, *ACS Catal.* **2021**, *11*, 7144–7153.
[62] R. A. Vicente, I. T. Neckel, P. S. Fernández, *ACS Electrochemistry* **2025**, *1*, 286-293.

[63] J. Zhang, W. K. Lee, M. Ge, *Commun. Mater.* **2022**, *3*, 1–9.
[64] Y. Huang, S. Wang, Y. Guan, A. Maier, *J. Synchrotron Radiat.* **2020**, *27*, 477–485.
[65] S. Czioska, A. Boubnov, D. Escalera-López, J. Geppert, A. Zagalskaya, P. Röse, E. Saraçi, V. Alexandrov, U. Krewer, S. Cherevko, J. D. Grunwaldt, *ACS Catal.* **2021**, *11*, 10043–10057.
[66] M. van der Merwe, R. E. Wibowo, C. E. Jimenez, C. Escudero, G. Agostini, M. Bär, R. Garcia-Diez, *ACS Catal.* **2024**, *14*, 16759–16769.
[67] M. Holler, A. Diaz, M. Guizar-Sicairos, P. Karvinen, E. Färm, E. Härkönen, M. Ritala, A. Menzel, J. Raabe, O. Bunk, *Sci. Rep.* **2015**, *4*, 3857.
[68] J. Foster, X. Lyu, A. Serov, S. Mauger, E. Padgett, S. Pylypenko, *Electrochim. Acta* **2025**, *517*, 145705.
[69] T. Seip, J. K. Lee, M. Ge, W. K. Lee, N. Shaigan, M. Dinu, K. Fatih, A. Bazylak, *Electrochim. Acta* **2023**, *462*, 142701.
[70] M. Holler, M. Odstrcil, M. Guizar-Sicairos, M. Lebugle, E. Müller, S. Finizio, G. Tinti, C. David, J. Zusman, W. Unglaub, O. Bunk, J. Raabe, A. F. J. Levi, G. Aeppli, *Nat. Electron.* **2019**, *2*, 464–470.
[71] M. Möckl, M. F. Ernst, M. Kornherr, F. Allebrod, M. Bernt, J. Byrknes, C. Eickes, C. Gebauer, A. Moskovtseva, H. A. Gasteiger, *J. Electrochem. Soc.* **2022**, *169*, 064505.
[72] H. Jang, J. Lee, *J. Energy Chem.* **2020**, *46*, 152–172.
[73] M. Holler, M. Odstrčil, M. Guizar-Sicairos, M. Lebugle, U. Frommherz, T. Lachat, O. Bunk, J. Raabe, G. Aeppli, *J. Synchrotron Radiat.* **2020**, *27*, 730–736.
[74] P. Bansal, N. Harjai, M. Saif, S. H. Mugloo, P. Kaur, *Neural Comput. Appl.* **2024**, *36*, 225–239.
[75] A. Romanowski, *IEEE Trans Industr Inform* **2019**, *15*, 1609–1618.
[76] Q. Xu, J. A. Zamora Zeledón, B. Ó. Joensen, L. Trotochaud, A. Sartori, L. M. Kaas, A. B. Moss, M. Mirolo, L. Mairena, S. Huynh, S. Garg, S. Helveg, I. Chorkendorff, S. Zhao, B. Seger, J. Drnec, *Nat. Nanotechnol.* **2025**, *2025*, 1–8.
[77] L. Ostervold, A. S. Hoffman, D. Thompson, S. R. Bare, E. L. Clark, *ChemCatChem* **2024**, *16*, e202400072.
[78] Y. Fam, T. L. Sheppard, J. Becher, D. Scherhaufer, H. Lambach, S. Kulkarni, T. F. Keller, A. Wittstock, F. Wittwer, M. Seyrich, D. Brueckner, M. Kahnt, X. Yang, A. Schropp, A. Stierle, C. G. Schroer, J. D. Grunwaldt, *J. Synchrotron Radiat.* **2019**, *26*, 1769–1781.
[79] X. Duan, X. F. Ding, N. Li, F. X. Wu, X. Chen, N. Zhu, *Comput. Biol. Med.* **2023**, *165*, 107473.
[80] G. Wang, J. C. Ye, B. De Man, *Nature Machine Intelligence* **2020**, *2*, 737–748.
[81] D. P. Finegan, I. Squires, A. Dahari, S. Kench, K. L. Jungjohann, S. J. Cooper, *ACS Energy Lett.* **2022**, *7*, 4368–4378.
[82] J. Scharf, M. Chouchane, D. P. Finegan, B. Lu, C. Redquest, M. cheol Kim, W. Yao, A. A. Franco, D. Gostovic, Z. Liu, M. Riccio, F. Zelenka, J. M. Doux, Y. S. Meng, *Nat. Nanotechnol.* **2022**, *17*, 446–459.
[83] R. Lou Omongos, D. E. Galvez-Aranda, F. M. Zanotto, A. Vernes, A. A. Franco, *J. Power Sources* **2025**, *625*, 235583.
[84] E. Pastor, Z. Lian, L. Xia, D. Ecija, J. R. Galán-Mascarós, S. Barja, S. Giménez, J. Arbiol, N. López, F. P. García de Arquer, *Nat. Rev. Chem.* **2024**, *8*, 159–178.

Manuscript received: March 25, 2025
Revised manuscript received: July 4, 2025
Accepted manuscript online: July 11, 2025
Version of record online: ■■, ■■